Tectonophysics 629 (2014) 87–108

Contents lists available at ScienceDirect

Tectonophysics

journal homepage: www.elsevier.com/locate/tecto

Anisotropy of magnetic susceptibility *versus* lattice- and shape-preferred orientation in the Lac Tio hemo-ilmenite ore body (Grenville province, Quebec)

Olivier Bolle [a,*,1], Bernard Charlier [a,b], Jérôme Bascou [c], Hervé Diot [d], Suzanne A. McEnroe [e]

[a] Dpt. de Géologie, Université de Liège, Bd. du Rectorat – Bât. B20, B-4000 Sart Tilman, Belgium
[b] Institut für Mineralogie, Leibniz Universität Hannover, Callinstrasse 3, D-30167 Hannover, Germany
[c] Université de Lyon, Université Jean Monnet and UMR-CNRS 6524, Laboratoire Magmas et Volcans, 23 Rue du Dr P. Michelon, F-42023 Saint Etienne Cédex 02, France
[d] UMR CNRS 6112, Laboratoire de Planétologie et Géodynamique, Nantes & PST, Université de La Rochelle, Av. M. Crépeau, F-17042 La Rochelle Cédex 01, France
[e] Institutt for geologi og bergteknikk, NTNU, Sem Sælandsv 1, N-7491 Trondheim, Norway

ARTICLE INFO

Article history:
Received 31 May 2013
Received in revised form 20 December 2013
Accepted 10 January 2014
Available online 24 January 2014

Keywords:
Magnetic fabric
EBSD
Image analysis
Iron–titanium ore
Anorthosite

ABSTRACT

The Lac Tio hemo-ilmenite ore body crops out in the outer portion of the 1.06 Ga Lac Allard anorthosite, a member of the Havre-Saint-Pierre anorthosite suite from the Grenville province of North America. It is made up of ilmenitite (commonly with more than 95% hemo-ilmenite) associated with noritic lithologies and anorthosite. The present study compares the magnetic fabric of the ore body, as deduced from anisotropy of magnetic susceptibility (AMS) measurements, with the crystallographic and shape fabrics, obtained from lattice-preferred orientation (LPO) and shape-preferred orientation (SPO) measurements made using electron backscattered diffraction (EBSD) and 3D image analysis, respectively. Room-temperature hysteresis measurements, thermomagnetic curves and values of the bulk magnetic susceptibility reveal a magnetic mineralogy dominated by a mixed contribution of hemo-ilmenite and magnetite. The hemo-ilmenite grains display a LPO characterized by a strong preferred orientation of the basal (0001) plane of ilmenite along which hematite was exsolved. This LPO and the magnetic fabric fit well (angle between the crystallographic *c*-axis and the axis of minimum susceptibility ≤ ca. 15° for most samples), and the latter is thus strongly influenced by the hemo-ilmenite magnetocrystalline anisotropy. A magnetite SPO, concordant with the hemo-ilmenite LPO, may also influence and even dominate the magnetic fabric. The rock shape fabric is coaxial with the magnetic fabric that can thus be used to perform detailed structural mapping. Interpretation of the magnetic fabric and field structural data suggests that the Lac Tio ore body would be a sag point at the margin of the Lac Allard anorthosite, deformed by ballooning during the final stage of diapiric emplacement of the anorthosite body.

1. Introduction

The Lac Tio hemo-ilmenite ore body is situated to 36 km NNE of Havre-Saint-Pierre, a small town lying on the north shore of the Saint Lawrence estuary, in the Quebec province. This magmatic ilmenite deposit crops out in the 1.06 Ga Lac Allard anorthosite which is part of the Havre-Saint-Pierre anorthosite suite, one of many anorthosite–mangerite–charnockite–(rapakivi) granite (AMCG) suites that characterize the Late-Mesoproterozoic to Early-Neoproterozoic Grenville province of North America (Emslie, 1978). The ore body is the world's largest known hard-rock ilmenite deposit, with reserves estimated at ca. 138 Mt even after 60 years of mining exploitation (Charlier et al., 2010).

The magnetic properties of the Lac Tio ore body and other hemo-ilmenite deposits of the area were thoroughly studied in the 1950s and 60s (Carmichael, 1959, 1961, 1964; Hargraves, 1959; Hargraves and Burt, 1967), and recently reinvestigated by McEnroe et al. (2007) and Robinson et al. (2013). These works focused on the natural remanent magnetization of the hemo-ilmenite ores, that was first linked to the exsolved lamellae of antiferromagnetic hematite alone (*e.g.* Carmichael, 1959; Hargraves, 1959), before being shown to reside in a defect moment at the interfaces between the lamellae and the paramagnetic ilmenite host (McEnroe et al., 2007), following the theory of lamellar magnetism (*e.g.* Robinson et al., 2002). Preliminary data on the anisotropy of magnetic susceptibility (AMS) were also provided (Hargraves, 1959; McEnroe et al., 2007; Robinson et al., 2013), but with no detailed discussion on the magnetic fabric. It was, however, suggested by Hargraves (1959) and Robinson et al. (2013), on

* Corresponding author. Tel.: +32 4 3662260; fax: +32 4 3662921.
E-mail address: olivier.bolle@ulg.ac.be (O. Bolle).
[1] Research Associate from the F.N.R.S., Belgium.

0040-1951/$ – see front matter © 2014 Elsevier B.V. All rights reserved.
http://dx.doi.org/10.1016/j.tecto.2014.01.012

qualitative to quantitative grounds, that the AMS would arise from a lattice-preferred orientation of the hemo-ilmenite grains.

The main goal of the present study is to analyze the geometric relationships between AMS and both lattice-preferred orientation (LPO) and shape-preferred orientation (SPO) of the rock-forming minerals, mainly hemo-ilmenite, in the Lac Tio ore body, in order to constrain the origin of the magnetic fabric and petrofabric of the deposit. To attain this objective, we have combined an AMS investigation of the deposit with hysteresis and thermomagnetic measurements, electron backscattered diffraction (EBSD) and 3D image analysis. As a conclusion, we propose a model of deformation of the Lac Tio hemo-ilmenite ore body.

2. Geological setting

2.1. The Havre-Saint-Pierre anorthosite suite

The Havre-Saint-Pierre anorthosite suite is a major component of the Saint-Jean domain (Fig. 1; Gobeil et al., 2003), a large, high-grade tectonostratigraphic unit that belongs to the allochthonous Medium Pressure Belt of the Grenville province (aM*P* Belt; Rivers et al., in press). The northern and eastern limits of the Saint-Jean domain are well-defined and correspond to major shear zones (Fig. 1): the 51st Parallel deformation corridor, to the north, that separates the Saint-Jean domain from the Lac-à-l'Aigle domain (another high-grade unit belonging also to the aM*P* Belt; Rivers et al., in press), and the Romaine and Abbé-Huard shear zones, to the east, that separate the Saint-Jean domain from the Natashquan domain (a lower grade domain that represents a segment of the allochthonous Low Pressure Belt or a*LP* Belt; Rivers et al., in press).

The bounding shear zones of the Saint-Jean domain correspond to thrust structures along which dominantly NW-directed thrust movements have occurred (Madore et al., 1999; Verpaelst et al., 1999), prior to local extensional and/or strike–slip reworking (Gobeil et al., 2003; Indares and Martignole, 1993). Regional metamorphism in the Saint-Jean domain is associated with the NW thrusting and subsequent deformations, and reached middle-amphibolite- to granulite-facies conditions (*e.g.* Chevé et al., 1999; Gobeil et al., 1999). It peaked at 1083–1076 Ma and lasted until 1063–1047 Ma (U–Pb dating of metamorphic zircons and monazites from high-grade gneisses and rocks of the Havre-Saint-Pierre anorthosite suite; Wodicka et al., 2003). These ages correspond to the ca. 1.09–1.02 Ga Ottawan collisional orogenic phase of the Grenvillian orogeny (Rivers, 2008; Rivers et al., in press).

The Havre-Saint-Pierre anorthosite suite (ca. 11,000 km^2) can be subdivided into seven anorthosite plutons or lobes, including the Lac Allard anorthosite, that are separated by mangeritic envelopes and discontinuities interpreted as thrust structures (Fig. 1; Gobeil et al., 2003). U–Pb zircon crystallization ages determined on anorthosite and mangeritic rocks from this suite (Emslie and Hunt, 1990; Morisset et al., 2009; van Breemen and Higgins, 1993; Wodicka et al., 2003) reveal two magmatic pulses, at ca. 1.13 Ga and ca. 1.06 Ga, respectively. These pulses can be ascribed to two periods of AMCG magmatism that

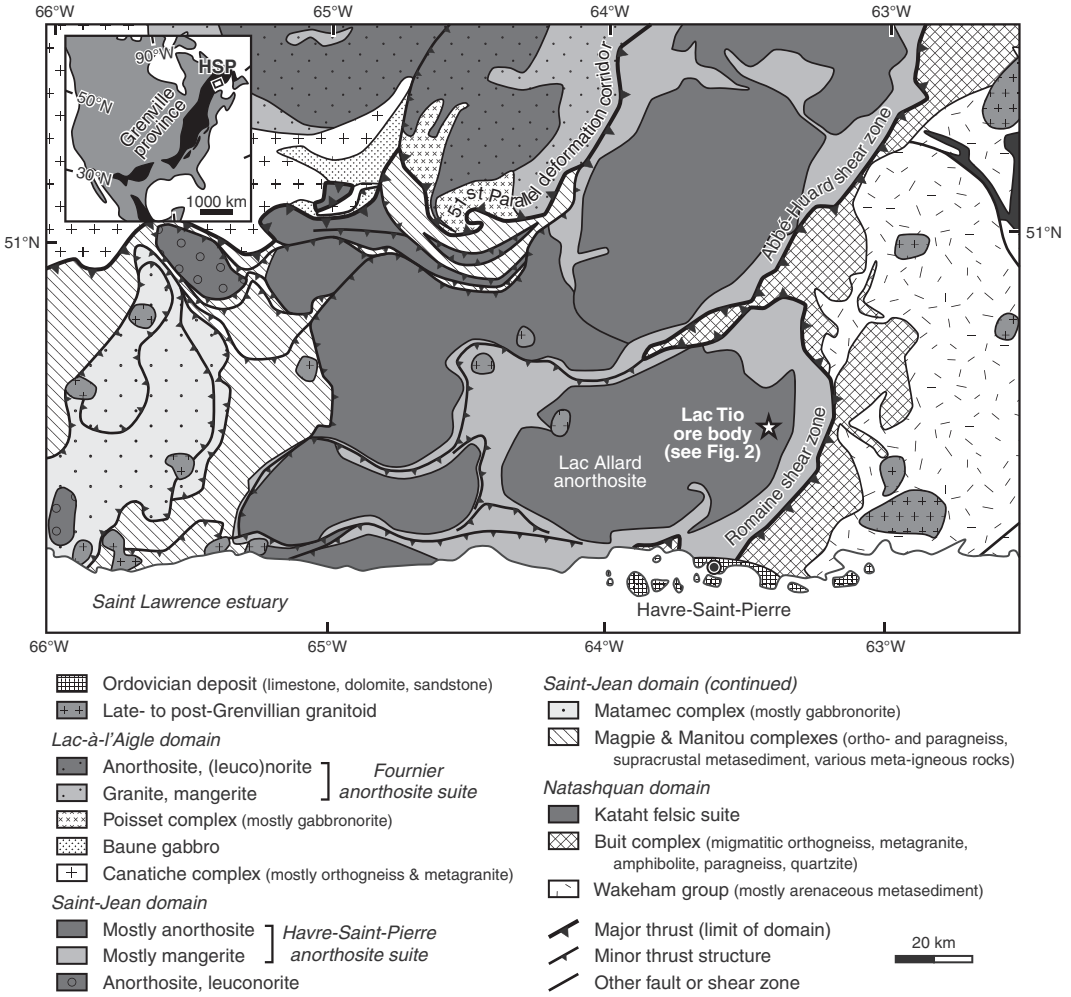

Fig. 1. Geological map of the Havre-Saint-Pierre anorthosite suite (simplified after Gobeil et al., 2003). Inset: Sketch map of the Grenville province of North America (simplified after Tollo et al., 2004), with location of the Havre-Saint-Pierre anorthosite suite (HSP).

have been recognized throughout the Grenville province (Hébert et al., 2005; Higgins and van Breemen, 1996; McLelland et al., 2010): the oldest period (ca. 1.16–1.13 Ga) pre-dated the Grenvillian orogeny and the youngest period (ca. 1.08–1.045 Ga) is syn-Ottawan.

2.2. The Lac Allard anorthosite

The Lac Allard anorthosite forms a complex, E–W to WSW–ENE elongated dome (ca. 70 km × 45 km), that is surrounded by a continuous, ca. 1–10-km-wide "mangeritic" rim made up of jotunite, (quartz) mangerite, charnockite and other granitoids (Fig. 1; Hocq, 1982). The dominant rock facies in the anorthosite dome is an andesine anorthosite (An_{37-50}; Charlier et al., 2008, 2010; Dymek, 2001; Hargraves, 1962; Hocq, 1982), that rarely contains more than 5% of mafic minerals (mainly orthopyroxene, clinopyroxene, Fe–Ti oxides). This anorthosite is partly to completely dynamically recrystallized into a millimetric plagioclase-rich matrix containing scattered, up to 20–30 cm plagioclase (and locally high-alumina orthopyroxene) porphyroclasts (Bergeron, 1986; Hargraves, 1962; Hocq, 1982). Minor zones of leuconorite, norite and gabbroic lithologies, as well as several-hectometers-wide sheets of oxide-apatite-gabbronorite occur locally (Bergeron, 1986; Dymek, 2001; Hargraves, 1962; Hocq, 1982).

The dome-shaped structure of the Lac Allard anorthosite is defined by the concentric arrangement of two subparallel planar structures (Hocq, 1982): (1) an igneous layering underlined by an igneous lamination of the plagioclase porphyroclasts (S_0; displayed only locally) and (2) a foliation defined by the shape-preferred orientation of small aggregates of mafic minerals and/or plagioclase porphyroclasts (S_1; very common). Gneissic or mylonitic foliation, as well as mega- to mesoscopic (overturned?) folds with axial plane foliation (S_2, defined in the same way as S_1) occur locally (Hocq, 1982).

The emplacement of the Lac Allard anorthosite has been dated at 1060 Ma, based on U–Pb zircon ages obtained on three distinct anorthosite samples (Morisset et al., 2009). The crystallization age of the mangeritic envelope of the anorthosite body would be older (1126 +7/−6 Ma; U–Pb zircon age; Emslie and Hunt, 1990). The Lac Allard anorthosite is thus related to the ca. 1.06 Ga syn-Ottawan AMCG magmatic pulse and intruded a mangeritic unit, emplaced earlier during the ca. 1.13 Ga pre-Grenvillian AMCG magmatic pulse and forming now a rim around the anorthosite body. These geochronological data imply also that the Lac Allard anorthosite emplaced in a hot, thickened orogenic crust, following or near the end of the Ottawan metamorphic peak (ca. 1080 Ma in the Saint-Jean domain; Wodicka et al., 2003; ca. 1090–1050 Ma at the scale of the aMP Belt; Rivers, 2008; Rivers et al., in press). This is consistent with very slow cooling rates estimated by Morisset et al. (2009) for the anorthosite (3–4 °C/Ma).

3. Structure, composition and origin of the Lac Tio ore body

3.1. From 2D to 3D description

The Lac Tio hemo-ilmenite ore body crops out on the eastern flank of the Lac Allard anorthosite dome (Fig. 1), where the S_0–S_1 structure is, in average, NNE–SSW-striking with dips of 15–80° to the east (Bergeron, 1986; Hargraves, 1962; Hocq, 1982). It consists of a main ore body (the Tio deposit *sensu stricto*) and two satellite Fe–Ti deposits, namely the North-West and Cliff deposits (Bergeron, 1986; Hammond, 1952), that are both separated from the main ore body by a septum of barren anorthosite (Fig. 2a). A small, discontinuous noritic unit showing a conspicuous igneous layering (here referred to as "layered norite") is locally observed along the eastern margin of the main ore body (Fig. 2a). This unit has been treated as a peculiar, minor rock facies of the ore body by Charlier et al. (2010).

The three portions of the deposit are elongated along a N–S to NNE–SSW direction in map view (Fig. 2a). The main ore body, as it crops out nowadays in the open pit, is 990 m in length and 820 m in width (Fig. 2a). Its thickness ranges from 60 to 360 m (based on the mining borehole database used to construct Fig. 2b, c). The North-West and Cliff deposits are 545 m × 345 m and 380 m × 225 m, with a thickness of 40–100 m and 60 m, respectively. The main ore body and the Cliff deposit are both dominantly east-dipping bodies (10–15° to 30°E), with a gently-dipping to flat-lying irregular floor, and moderately- to steeply-dipping, locally overturned eastern, northern and southern flanks (Fig. 2b, c). The North-West deposit has a well-defined basin shape. The layered norite is interbedded at the roof of the main ore body.

The Lac Tio ore body and the host anorthosite are cut by joints and normal faults that are striking NNW–SSE to NE–SW and have steep dips (usually to the east) to vertical attitude (Fig. 2a; Hammond, 1952). Following Hammond (1952), the eastern part of the ore body has been moved downwards over a distance of ca. 90 m, along a major N–S, steeply-dipping normal fault that "cuts through the middle of the deposit". Such an important slip is not supported by our analysis of the mining borehole database. The potential displacement induced by other normal faults is unknown, but probably not important.

3.2. Lithology

The ore body is composed of rocks essentially made up of hemo-ilmenite (*i.e.* ilmenite with exsolved hematite lamellae) and plagioclase in various proportions, namely ilmenitite, norite and anorthosite. Ilmenitite is the dominating rock facies. It is coarse-grained (up to 15–20 mm) and alternates with the more leucocratic rocks that form, at the scale of the ore body, several-decameters-thick layers and lenses which are irregularly distributed (Bergeron, 1986; Charlier et al., 2010; Hammond, 1952). Such an alternation between rocks variably enriched in hemo-ilmenite is observed down to the centimeter scale. The ore (ilmenitite and ilmenite-rich norite) has an exceptionally high content in hemo-ilmenite (66.2 wt.% on average, with half of the ore that contains more than 76.3 wt.% hemo-ilmenite; Charlier et al., 2010).

3.3. Macrostructures

At the outcrop scale, alternations of plagioclase-rich (hemo-ilmenite-poor) and plagioclase-poor (hemo-ilmenite-rich) layers define an igneous layering in the ore body (Fig. 3b). Layer-parallel igneous lamination of the plagioclase is common, as well as a flattening of variable degree of the hemo-ilmenite grains, usually also parallel to the igneous layering. Some measurements of the layering orientation do not reveal any obvious pattern in the deposit (Fig. 2a). However, at a larger scale, the internal structure of the ore body, as shown by norite and anorthosite layers and lenses, is broadly parallel to the contact with the host anorthosite (Bergeron, 1986; Charlier et al., 2010; Hammond, 1952). Igneous lamination of plagioclase and orthopyroxene, as well as modal layering, is present in the layered norite.

The anorthosite layers that define the layering in the ore body are commonly "disrupted" (stretched), forming fragments (boudins) that have tapered or angular tips in cross section (Fig. 3a, b). These anorthosite fragments are still aligned in the layering plane or have been slightly moved, and they are separated from each other by ilmenitite or norite material. Moreover, the layering is locally affected by meter-scale isoclinal slump folds. All these features point to the gravitational sliding of a poorly consolidated crystal mush, during collapse of the crystallizing heavy ore body into the lower density host rocks (Glazner and Miller, 1997), a feature reported for a number of mafic to ultramafic igneous bodies worlwide (*e.g.* Bolle et al., 2002; McBirney and Nicolas, 1997; O'Driscoll et al., 2007). A later deformation phase is evidenced by the local occurrence of upright, gentle folds with decametric wavelength and amplitude that affect stretched anorthosite layers (Fig. 3a).

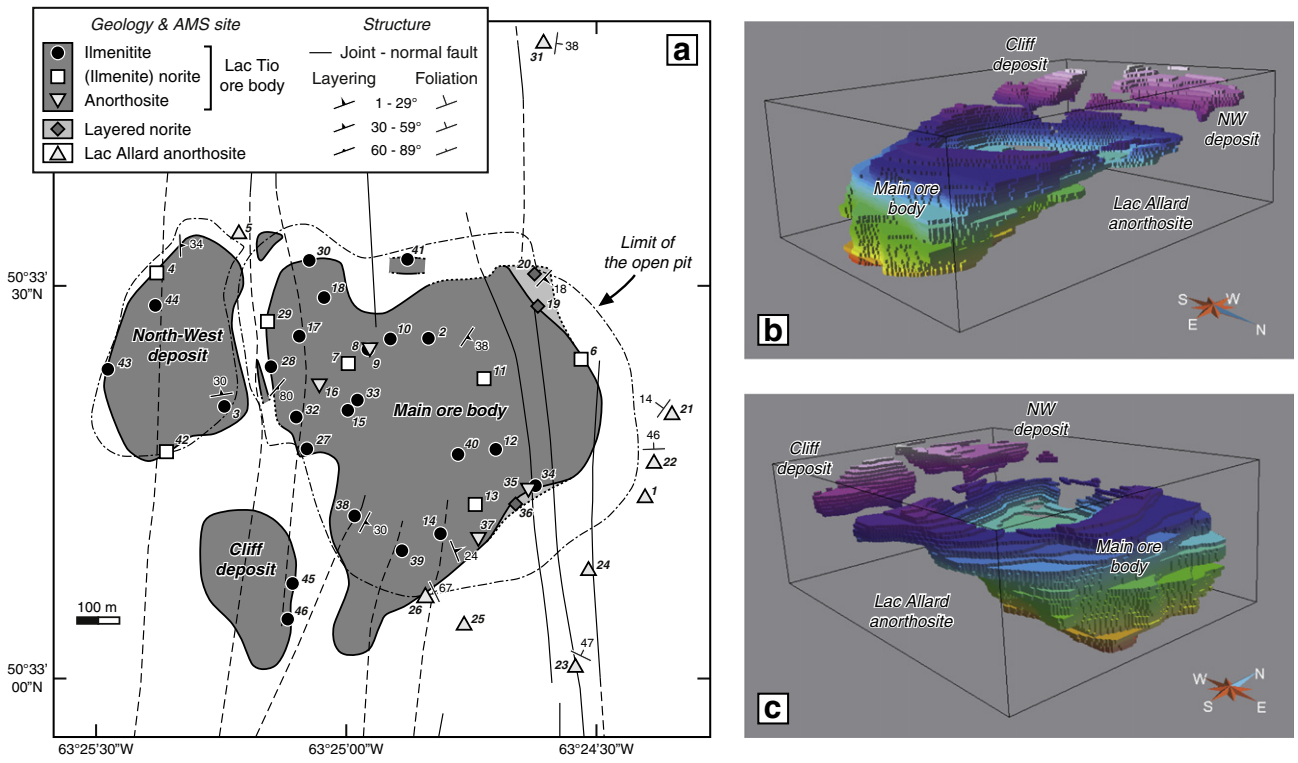

Fig. 2. (a) Simplified geological map of the Lac Tio ore body, with location of the sampling sites. Stippled lithological limits, joints and faults are hypothetical. Limits of the ore body (modified by the mining operations) and that of the pit are drawn, as they were in the mid 2000s, using mining data provided by QIT-Fer et Titane Inc. Joint and fault traces are drawn from lineaments evidenced on air photographs (Fig. 2 of Hammond, 1952 and Google Earth© image) and from whitened (weathered) zones observed in the pit. The fracture traces evidenced on old air photographs were adapted, where possible, to fit modifications of the topography induced by the mining operations. Barren rock dumps covering the host anorthosite to the north and east of the mine are not represented. Layering: igneous layering, as measured in the ore body; foliation: S_0–S_1 structure, as measured in the Lac Allard anorthosite (see text for more explanations). Anorthosite samples collected in the main ore body (TL9, TL16, TL35, TL37) come from thin layers interbedded in the ore, except TL16 which is from a large anorthositic body at the bottom of the main pit and that corresponds either to a thick layer or lens, or to a shelf of wall-rocks. (b–c) 3D shape reconstruction of the Lac Tio ore body based on the geochemical composition of 172,643 samples from boreholes (mining database provided by QIT-Fer et Titane Inc.), using the GOCAD© software (from Charlier et al., 2010). Color scale is for depth.

3.4. Petrogenesis

The Lac Tio ore body has been long interpreted as an immiscible Fe–Ti-rich liquid derived from a parent ferrodioritic (=jotunitic) magma (Force, 1991). However, based on whole-rock and mineral chemical data (Charlier et al., 2010), the hemo-ilmenite deposit has been shown to have a cumulate origin, formed through multiple emplacements of ferrobasaltic magma, alternating with magma hybridization and fractional crystallization. It has also been suggested by Charlier et al. (2010) that the ore body was not a slowly cooled magma chamber,

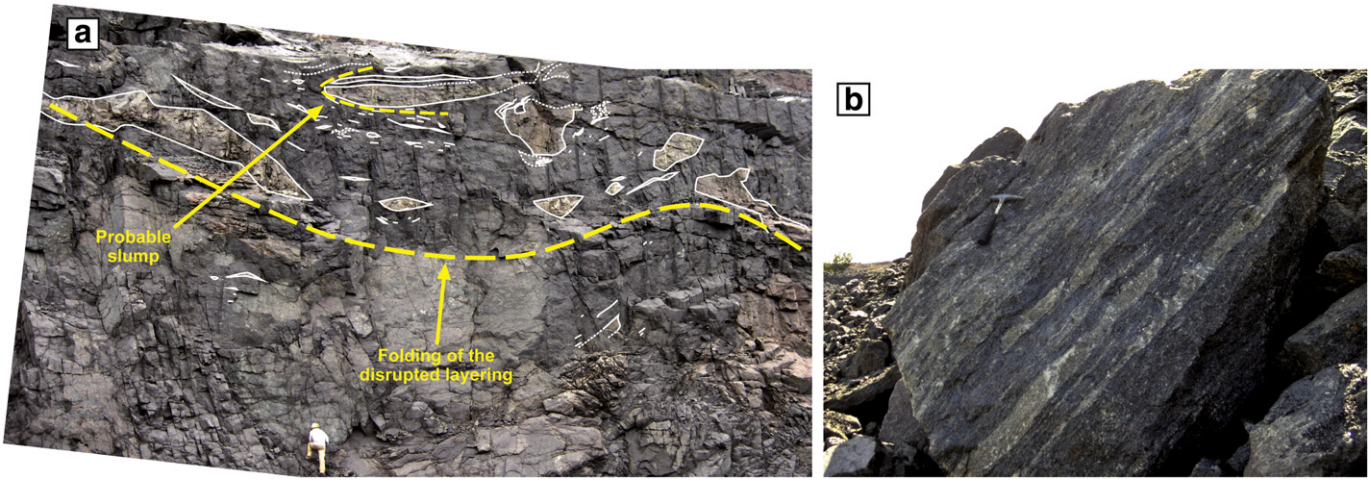

Fig. 3. (a) "Disrupted" (stretched) anorthosite layers affected by upright, gentle folds (western flank of the main pit, above sample TL28; see Fig. 4 for location); (b) Igneous layering defined by the alternance of hemo-ilmenite-rich layers and anorthosite layers. The anorthosite layers are locally stretched, which confers an irregular appearance to the layering (erratic block left after mining operations, North-West deposit).

but rather a magma conduit in which density-driven accumulation of hemo-ilmenite and possibly plagioclase buoyancy occurred, explaining the huge concentration of hemo-ilmenite.

4. Sampling and microscopic features

4.1. Sampling

A total of 46 samples have been collected in the open pit and its surroundings, following a grid that was strongly dependent on the access and outcrop conditions (Fig. 2a). The samples consist of blocks that have been oriented using a clinometer and a home-made sun compass, because of the strong magnetization of the ore body.

Nine samples come from the host anorthosite (TL01, TL05, TL21 to TL26, TL31), three from the layered norite (TL19–20, TL36) and thirty-four from the ore body (twenty-seven samples are from the main ore body, five from the North-West deposit and two from the Cliff deposit). These samples range from ilmenitite (commonly with more than 95% hemo-ilmenite) to anorthosite, through hemo-ilmenite-plagioclase lithologies (here called norite or ilmenite norite, depending if they contain some orthopyroxene or not, following the simplified terminology of Charlier et al., 2010).

In the laboratory, 25-mm-diameter oriented cores were drilled in the samples, using a standing drill. These cores were further cut into 22-mm-high cylinders, hence providing 205 specimens (usually four per oriented sample) for the AMS measurements.

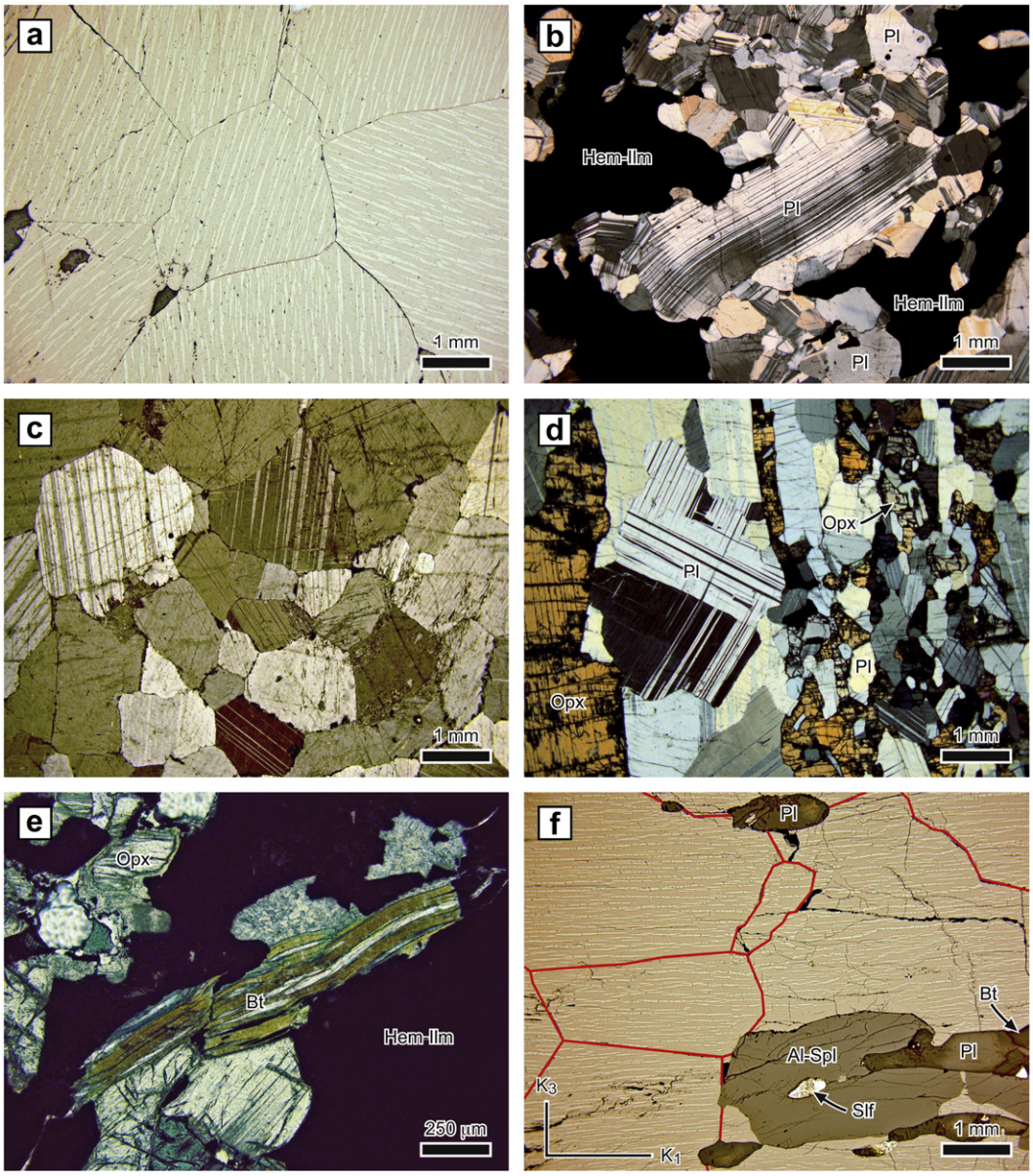

Fig. 4. Photomicrographs of various microstructures. (a) Recrystallized polygonal hemo-ilmenite grains, with boundaries tending to make triple junctions at ca. 120° (ilmenitite TL18; reflected light, crossed nicols); (b) large plagioclase grain showing curved polysynthetic twins, fringed with aggregates of small plagioclase grains (probable porphyroclast and new, recrystallized grains) and associated with hemo-ilmenite areas (ilmenite norite TL42; transmitted light, crossed nicols); (c) recrystallized mosaic of plagioclase grains, with local triple junctions at ca. 120° (deposit anorthosite TL09; transmitted light, crossed nicols); (d) strong SPO of plagioclase and orthopyroxene grains (note the abrupt decrease of grain size from left to right; layered norite TL20; transmitted light, crossed nicols); (e) biotite kinking (norite TL07; transmitted light, uncrossed nicols); (f) strong SPO of hemo-ilmenite grains and their exsolution lamellae, as well as all other rock-forming minerals in a section cut parallel to the K_1K_3 AMS plane (note flattening perpendicular to the K_3 axis and lengthening parallel to K_1; ilmenitite TL03; reflected light, crossed nicols; the boundaries of the hemo-ilmenite grains are highlighted in red). Symbols for minerals: Al-Spl, aluminous spinel; Bt, biotite; Hem-Ilm, hemo-ilmenite; Opx, orthopyroxene; Pl, plagioclase; Slf, unspecified sulfide (chiefly pyrite).

4.2. Petrography

The petrography of our samples is summarized below. Details on the opaque mineralogy are given in e-Table 1 (Appendix A).

The ilmenitites and ilmenite-plagioclase lithologies (Fig. 4a, b, f) are coarse-grained (ca. 2–11 mm in average), their texture evolving from anhedral to subhedral granular with increasing plagioclase proportions. They are made up of hemo-ilmenite, andesine plagioclase (as a main or accessory mineral, depending on the lithology) and various accessory minerals: aluminous spinel, biotite (Ti-phlogopite; Charlier et al., 2010), sulfides (pyrite and chalcopyrite, some Ni–Co sulfides, including millerite, and sporadic traces of pyrrhotite), and, in a few samples, magnetite, hypersthene and/or apatite. The hemo-ilmenite grains display several generations of exsolutions of decreasing size (Fig. 5a), down to the nanometer scale (McEnroe et al., 2007), the optically visible hematite lamellae forming ca. 30% of the grains (Bergeron, 1986; McEnroe et al., 2007). Some hemo-ilmenite grains contain lamellae of magnetite parallel to the hematite exsolutions, and with a size of the same order as the first-generation hematite plates (a few tens of μm; Fig. 5c). They are observed in many samples (e-Table 1), but always in minor amounts (bulk proportions ≤ ca. 1–1.5%). These lamellae would result from a high-temperature, localized reduction–exsolution process that preceded the lower temperature, standard exsolutions of hematite (Robinson et al., 2013). Plagioclase is locally slightly micro-antiperthitic and contains abundant oriented inclusions (mainly needles and plates of rutile, (ilmeno-)hematite and (hemo-)ilmenite). Aluminous spinel forms quite large, commonly zoned external granule exsolutions along the margin of hemo-ilmenite crystals, as well as exsolved lenses and

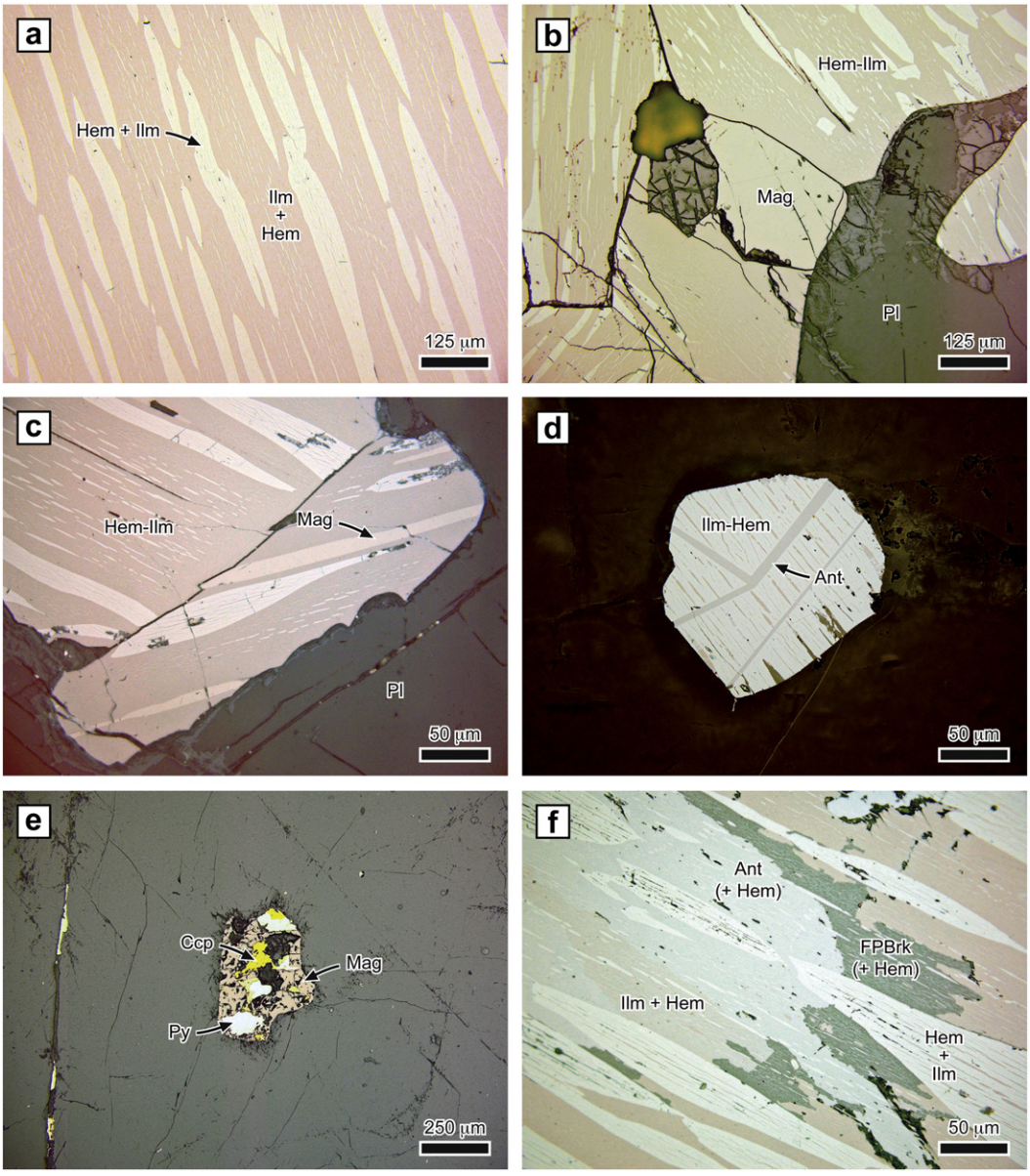

Fig. 5. Photomicrographs illustrating various microscope-scale features in the opaque phases (reflected light, crossed or – for Fig. 6b, e – uncrossed nicols). (a) Typical hemo-ilmenite displaying large exsolution lamellae of hematite (a few tens of μm) and a second, subsequent generation of thinner hematite exsolution lamellae (≤1 mm), both formed parallel to the (0001) plane of the host ilmenite (note the small ilmenite exsolutions in the first-generation hematite lamellae; ilmenitite TL32); (b) primary, interstitial grain of magnetite (note the decreasing amount and size of hematite lamellae in hemo-ilmenite towards the boundaries of the magnetite grain; ilmenite norite TL13); (c) lamellae of magnetite in hemo-ilmenite grains (ilmenite norite TL13); (d) ilmeno-hematite grain with lamellae of anatase (Lac Allard anorthosite TL25); (e) composite sulfide grain (pyrite + chalcopyrite) included in plagioclase, with pyrite partly transformed to magnetite (note the microfracture filled with sulfide, to the left of the micrograph; ilmenitite TL40); (f) anatase and possible "ferropseudobrookite" arising from the partial alteration of the ilmenite host in hemo-ilmenite grains (ilmenitite TL34). Symbols for minerals: Al-Spl, aluminous spinel; Ant, anatase; Ccp, chalcopyrite; FPBrk, "ferropseudobrookite"; Hem, hematite; Hem-Ilm, hemo-ilmenite; Ilm, ilmenite; Ilm-Hem, ilmeno-hematite; Mag, magnetite; Pl, plagioclase; Py, pyrite.

granules in these crystals. Biotite is usually found as flakes, at the contact between plagioclase and hemo-ilmenite. Samples TL06, TL07, TL13 and TL28 contain interstitial grains of magnetite, in minor amounts (Fig. 5b; e-Table 1). Hypersthene and very minor amounts of apatite are observed in samples TL07, and TL08 and TL28, respectively, mostly as subhedral prismatic grains.

Samples from the Lac Allard anorthosite exhibit an anhedral granular mosaic of plagioclase grains (ca. 1.5–8.5 mm in average). Plagioclase is micro-antipertithic and contains abundant, minute inclusions of rutile and Fe–Ti oxides, as in ilmenitites and (ilmenite) norites. Interstitial grains of mafic minerals are scarce (<5%, with the notable exception of sample TL26) and consist of hypersthene, diopside, opaque phases (ilmeno-hematite and hemo-ilmenite, with subordinate amounts of magnetite and traces of pyrite, chalcopyrite and pyrrhotite), green hornblende and biotite. Ilmeno-hematite grains exhibit locally lamellae of anatase (probable oxidation texture; Fig. 5d). Myrmekites are found at plagioclase grain boundaries. Samples collected in anorthosite layers of the ore body are petrographically similar to those from the host anorthosite (Fig. 4c); however, they do not contain clinopyroxene and are less rich in myrmekites.

Samples from the layered norite are coarse-grained (ca. 5 mm in average) and display a subhedral granular texture (Fig. 4d). They are mainly made up of plagioclase, hypersthene and hemo-ilmenite, which exhibit the same textural features as noritic samples from the ore body, except that plagioclase is markedly micro-antiperthitic, and that hypersthene shows regular plates of hemo-ilmenite (Schiller texture) and thin lamellae of clinopyroxene, both exsolved parallel to (100). Flakes of biotite at the contact between plagioclase and hemo-ilmenite, diopside as isolated grains or external exsolution granules at the border of orthopyroxene crystals, and interstitial grains of magnetite and sulfides (mostly pyrite, plus some chalcopyrite and pyrrhotite) are also observed.

A limited alteration of primary silicates is expressed by minor amounts of sericite, epidote calcite and chlorite, arising mainly from the transformation of plagioclase and biotite. Grains of Fe-sulfides are commonly partly to completely replaced by magnetite (Fig. 5e; e-Table 1). Local transformation of the primary oxide phases gave rise to either patchy areas of Ti-rich secondary minerals formed at the expense of the ilmenite component in hemo-ilmenite and ilmeno-hematite (anatase associated locally with possible "ferropseudobrookite"; see the discussion in Sakoma and Martin, 2002; Fig. 5f; e-Table 1) or, except in anorthosite samples, small grains of an Fe-rich secondary phase arising from the alteration of the hematite component in hemo-ilmenite (lepidocrocite?; e-Table 1). Secondary magnetite and sulfides are also found as filling in microfractures and grain boundaries (Fig. 5e).

4.3. Microstructures

All sampled lithologies display microscale evidence of ductile deformation and recrystallization. Intracrystalline deformation is attested by undulose extinction or subgrains and/or bending of polysynthetic twins in plagioclase (Fig. 4b), as well as bending or kinking of orthopyroxene and biotite crystals (Fig. 4e). In the Lac Allard anorthosite, deformation of the minerals is weak and concerns mainly some of the largest grains of plagioclase that can be interpreted as porphyroclasts isolated in a recrystallized groundmass (Hocq, 1982). This also applies to the anorthosite layers sampled in the ore body. Intracrystalline deformation of silicates is more intense in ilmenitites and noritic samples. However, in these rocks, deformation of plagioclase (and orthopyroxene, where present) is widespread only in large, subhedral crystals, whereas small anhedral grains of these minerals, that form relatively equigranular aggregates associated with the subhedral crystals, show only sporadic evidence of intracrystalline deformation (Fig. 4b). The former minerals correspond to porphyroclasts, whereas most of the small aggregated grains would be new grains developed by dynamic recrystallization (likely through subgrain rotation; *e.g.* Passchier and Trouw, 2005).

The hemo-ilmenite grains in ilmenitites and noritic samples are typically polygonal, with boundaries tending to make triple junctions with interfacial angles of approximately 120° (Fig. 4a). Such a grain shape is typical of an annealing texture resulting from static recrystallization (also called textural equilibration in igneous rocks; *e.g.* Higgins, 2011). Following Charlier et al. (2010), static recrystallization of the Lac Tio ore body occurred during the slow cooling of the host anorthosite (3–4 °C/Ma; Morisset et al., 2009), and is coeval with exsolution of the aluminous spinel that further reacted with hypersthene to form high-alumina orthopyroxene and sapphirine (not observed in our samples). A textural coarsening (*e.g.* Higgins, 2011) of the hemo-ilmenite was produced by this recrystallization, as shown by the smaller size of hemo-ilmenite grains that are included in plagioclase (grains preserved from recrystallization) or that form mosaic arrangements between plagioclase grains (coarsening hindered by the plagioclase boundaries). Equilibration of grain boundaries is rare for silicates and seems to concern only plagioclase grains formed through dynamic recrystallization (120° triple junctions are displayed locally, in the aggregates of small plagioclase grains observed in ilmenitites and noritic samples, and in the plagioclase-rich matrix of anorthosites; Fig. 4c). This observation, together with the preservation of intracrystalline deformation microstructures in the silicates indicates that the latter have been much less affected by static recrystallization than hemo-ilmenite, which reflects the aptitude of Fe–Ti oxide minerals for recrystallizing (see discussion in Duchesne, 1999).

Despite the static recrystallization, the hemo-ilmenite grains still commonly display a slight to strong SPO (Fig. 4f), with a flattening plane usually parallel to the igneous lamination of the plagioclase (plus orthopyroxene in the layered norite; Fig. 4d) that was formed during emplacement and crystallization in the host anorthosite. The hematite exsolution lamellae of the hemo-ilmenite grains display a slight to strong SPO, parallel to the SPO of the grains where the latter is expressed (Fig. 4f).

5. Rock magnetic study

Extensive high- and low-temperature rock-magnetic, and Mössbauer experiments were made by McEnroe et al. (2007), on a set of Hargraves original samples from the Lac Tio ore body and other hemo-ilmenite deposits from the area, which we use as additional background for our interpretations. Here, we focus on new hysteresis and thermomagnetic analyses, to constrain better the interpretation of the AMS data.

Hysteresis and high-temperature measurements were made, on chips (10–30 mg) taken from core fragments after cutting the AMS cylinders, on a Princeton vibrating sample magnetometer (VSM) from Princeton Instruments. Hysteresis loops were measured at room-temperature, in a maximun field of 1 T. High-temperature measurements were made with the furnace installed in the VSM, using the method of Fabian et al. (2013). Here, a sequence of saturation-initial curves $M_{si}(H, T)$ from room-temperature is measured with increasing temperature in an interval of 3 °C to a maximum temperature of 720 °C, in approximately 230 steps. At each temperature step, T_i to T_{i+1}, the sample is heated in zero field to T_{i+1}. The field was then increased in steps of 50 mT to a maximum field of 1 T. Using this method, four parameters are measured: saturation magnetization, saturation remanence, initial or low-field magnetic susceptibility and high-field magnetic susceptibility for each temperature step. There is an approximate ± 5 °C error in the measurements.

5.1. Hysteresis measurements

Room-temperature hysteresis measurements were made on chips from eight samples: three ilmenitites (TL17, TL34 and TL43) and three (ilmenite) norites (TL06, TL07 and TL13), plus one layered norite (TL36) and one sample form the Lac Allard anorthosite (TL24). The

selected samples are representative of the different rock types and oxide mineralogies (e-Table 1), and their bulk magnetic susceptibility values, as calculated from the AMS data presented later, cover the susceptibility range of the entire sample set (Table 2). A high-field slope correction has been applied to the hysteresis measurements. A selection of adjusted hysteresis loops is shown in Fig. 6 and values of the hysteresis parameters (coercivity of remanence, H_{cr}; coercivity, H_c; saturation remanence, M_{rs}; saturation magnetization, M_s; and the corresponding ratios H_{cr}/H_c and M_{rs}/M_s) are given in Table 1. In this table, TL13-1, TL13-2 and TL34-1, TL34-2 correspond to two measurements made on different fragments from the same core.

Ilmenitites TL17 and TL34, which contain negligible or no magnetite (*i.e.* a maximum of one grain of primary magnetite or one area of secondary magnetite replacing sulfide was detected per thin section, and magnetite lamellae were not observed in the hemo-ilmenite grains), have the highest coercivity (H_c) values (>100 mT; Table 1) and wide adjusted hysteresis loops (Fig. 6a). These hysteresis data are dominated by the high-coercivity hemo-ilmenite grains. The other selected samples from the ore body, as well as layered norite TL36, contain primary and/or secondary magnetite in non-negligible amounts and have narrow hysteresis loops (Fig. 6b, c), reflecting the lower coercivity of the magnetite.

The hysteresis loops of the ilmenitites and noritic samples display variable degrees of constriction (Table 1; Fig. 6), from wide loops with no or slight constriction (TL17, TL34-1, TL34-2; H_{cr}/H_c = 1.0–1.5 and M_{rs}/M_s = 0.50–0.85), through moderately to strongly wasp-waisted loops (TL06, TL13-1, TL13-2, TL43; H_{cr}/H_c = 3.8–7.1 and M_{rs}/M_s = 0.15–0.36), to very narrow loops (TL07, TL36; H_{cr}/H_c = 3.3–3.8 and M_{rs}/M_s = 0.07–0.10). This reflects primarily an increasing contribution of low-coercivity magnetite *vs.* high-coercivity hemo-ilmenite from TL17, TL34-1 and TL34-2 (hemo-ilmenite-controlled hysteresis) to TL07 and TL36 (magnetite-controlled hysteresis). An additional effect on the hysteresis shape is the orientation of the hematite exsolution lamellae relative to the applied field. Indeed, it has been shown that hemo-ilmenite grains with hematite lamellae at high angle to the applied field display a much higher coercivity than grains with lamellae at low angle (McEnroe et al., 2007). Thus, the orientation of the rock fragment in the VSM influences the resulting hysteresis loop. This effect probably explains for example a small constriction in the hysteresis loop of TL34-1 (Table 1).

Sample TL24 from the Lac Allard anorthosite has the lowest magnetization values, resulting in a low M_{rs}/M_s ratio of 0.06 (Table 1), and very low H_{cr} and H_c values, giving a H_{cr}/H_c ratio of 3.9 (Table 1). The corresponding adjusted hysteresis loop is very narrow. These hysteresis data indicate a weak "ferro"magnetic (ferrimagnetic) behavior, carried by a very small amount of magnetite, in agreement with the opaque mineralogy of the host anorthosite (scarce oxides, including some grains of magnetite).

In a classical M_{rs}/M_s *vs.* H_{cr}/H_c plot (Day et al., 1977; Dunlop, 2002; Fig. 7), most data are trending from the single-domain to the pseudo-

Table 1
Hysteresis parameters.

Sample	Rock type	H_{cr}	H_c	M_{rs}	M_s	H_{cr}/H_c	M_{rs}/M_s
TL06	Ilmenite norite	32.4	7.9	118.0	792.8	4.1	0.15
TL07	Norite	19.3	5.1	171.3	2385	3.8	0.07
TL13-1	Ilmenite norite	200.8	28.4	74.4	204.9	7.1	0.36
TL13-2	Id.	29.9	7.8	167.4	858.6	3.8	0.19
TL17	Ilmenitite	187.7	179.6	90.9	106.8	1.0	0.85
TL24	Host anorthosite	26.1	6.7	2.1	35.2	3.9	0.06
TL34-1	Ilmenitite	170.9	111.1	87.0	175.7	1.5	0.50
TL34-2	Id.	193.0	178.1	68.8	92.3	1.1	0.75
TL36	Layered norite	20.3	6.1	58.8	563.2	3.3	0.10
TL43	Ilmenitite	231.7	45.1	58.5	174.8	5.1	0.33

H_{cr}: coercivity of remanence (in mT); H_c: coercivity (in mT); M_{rs}: saturation remanence (in mA·m^2/kg); M_s: saturation magnetization (in mA·m^2/kg).
All hysteresis parameters correspond to adjusted hysteresis loops after high-field slope correction.
TL13-1, TL13-2 and TL34-1, TL34-2 correspond to measurements made on two different fragments of the same core.

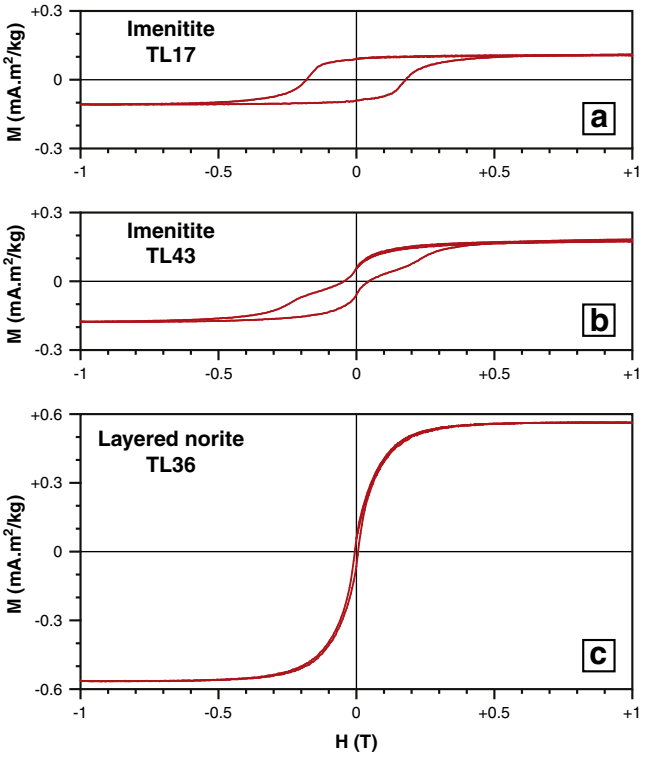

Fig. 6. Selected adjusted hysteresis loops after high-field slope correction, illustrating the increasing contribution to magnetization of low-coercivity magnetite *vs.* high-coercivity hemo-ilmenite. (a) Wide hysteresis loop (hemo-ilmenite-only loop; ilmenitite TL17); (b) moderately wasp-waisted hysteresis loop (minor magnetite contribution, mainly as lamellae of magnetite in the hemo-ilmenite grains; ilmenitite TL43); (c) very narrow hysteresis loop (magnetite-controlled loop, due to minor primary and secondary magnetite; layered norite TL36). *M*, magnetization; *H*, applied magnetic field.

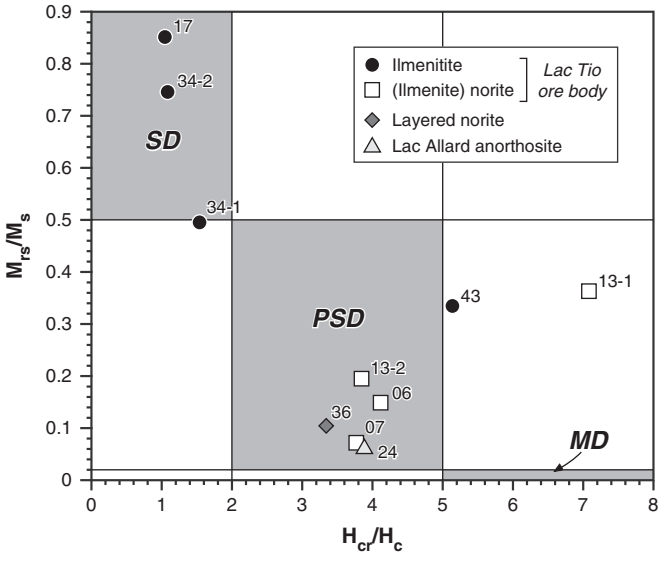

Fig. 7. M_{rs}/M_s *vs.* H_{cr}/H_c plot of Day et al. (1977), with limits between single-domain (SD), pseudo-single-domain (PSD) and multidomain (MD) grains after Dunlop (2002). H_{cr}, coercivity of remanence; H_c, coercivity; M_{rs}, saturation remanence; M_s, saturation magnetization. All hysteresis parameters after high-field slope correction. Note domain limits apply to magnetite only, not to hemo-ilmenite. However, the plot is used here to compare the samples which contain magnetite and those that have hemo-ilmenite as the sole oxide.

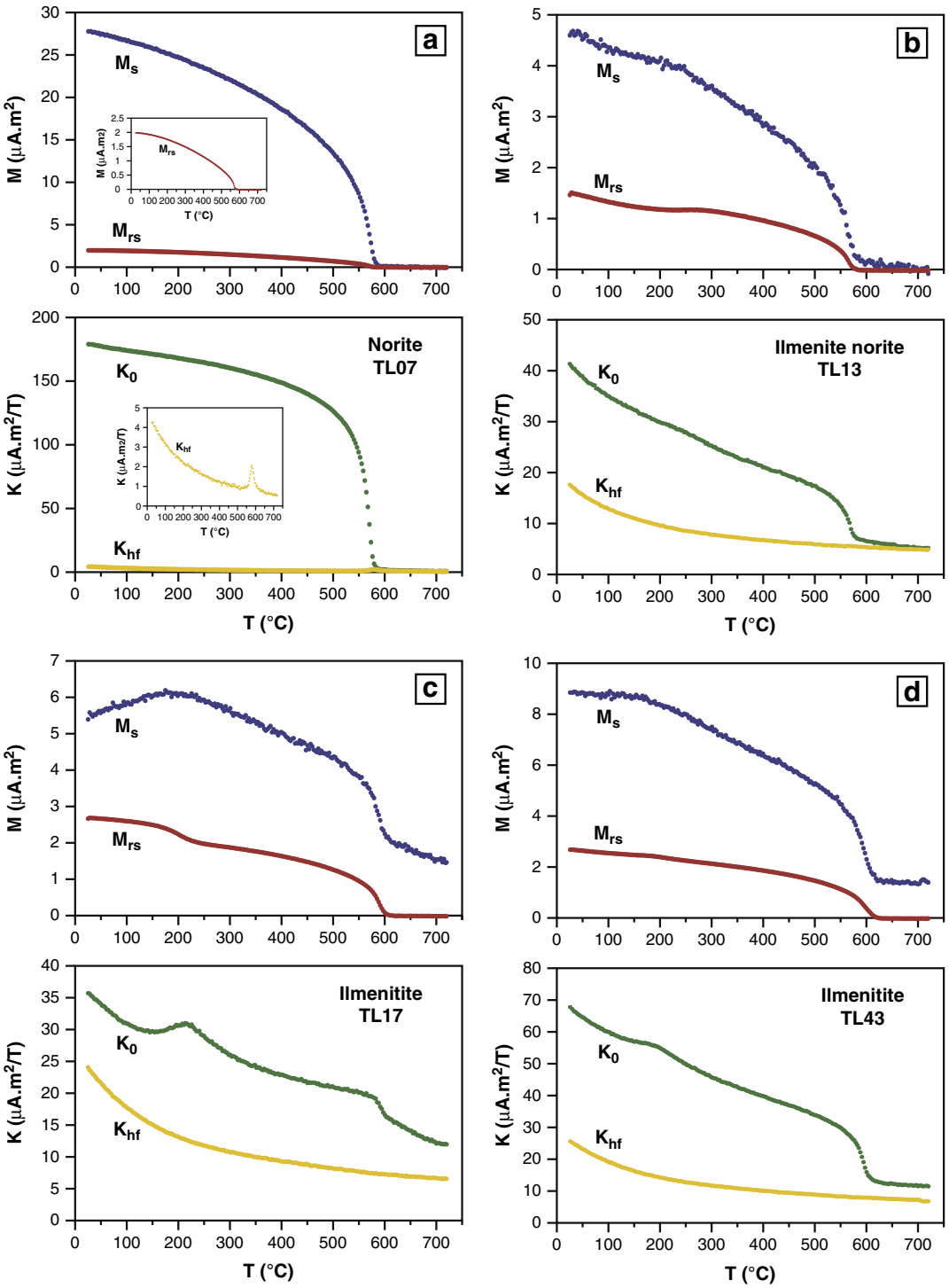

Fig. 8. High-temperature measurements using the method of Fabian et al. (2013), for (a) norite TL07 (relatively rich in sulfides and magnetite, respectively ca. 2%, as determined optically and ca. 2.5%, as calculated from the susceptibility values); (b) ilmenite norite TL13 (contains some primary and secondary magnetite); (c) ilmenitite TL17 (no magnetite detected optically); (d) ilmenitite TL43 (quite abundant magnetite lamellae in hemo-ilmenite grains, representing a maximum of ca. 1% of the bulk sample). The top panels show the extrapolated M_s *vs.* T calculated from a linear fit of the high field data and the approximate M_{rs} *vs.* T curves from the measured saturation-initial curves $M_{si}(H, T)$. The bottom panels contain the K_0 *vs.* T and K_{hf} *vs.* T curves inferred from the same data set. M_s, saturation magnetization; M_{rs}, saturation remanence; K_0, initial (or low-field) magnetic susceptibility; K_{hf}, high-field magnetic susceptibility. In Fig. 8a, the top inset is an enlarged $M_{rs}(T)$ curve and the bottom inset is an enlarged $K_{hf}(T)$ curve showing a Hopkinson peak for magnetite. Note the curves are not weight normalized and the vertical scales vary from one sample to another.

single-domain (PSD) area, the samples showing magnetite-dominated hysteresis loops (TL07, TL24, TL36; Table 1; Fig. 6c) being close to the PSD-multidomain (MD) boundary, which suggests a mixture of PSD and MD magnetite grain sizes.

5.2. Thermomagnetic measurements

Four samples investigated through the room-temperature hysteresis measurements have been selected for thermomagnetic analysis (TL07,

Table 2
AMS data.

Sample	n	X	Y	Z	Rock type	K_m	P_j	T_j	K_1				K_2				K_3			
									Dec	Inc	σ_1	σ_2	Dec	Inc	σ_1	σ_2	Dec	Inc	σ_1	σ_2
TL01	7	0471188	5600292	250	Host anorthosite	0.99	1.11	0.04	13	24	23	6	108	9	23	9	218	64	10	7
TL02	4	0470680	5600670	73	Ilmenitite	61.1	2.32	0.84	225	31	65	4	130	9	63	13	25	58	15	10
TL03	4	0470195	5600525	274	Ilmenitite	33.7	3.93	0.88	64	9	13	1	329	31	13	1	169	57	5	1
TL04	2	0470041	5600828	273	Ilmenite norite	17.3	1.19	−0.11	28	9	8	0	124	36	16	0	286	53	16	0
TL05	4	0470234	5600919	270	Host anorthosite	1.6	1.08	0.12	163	27	13	8	253	1	12	6	344	63	13	6
TL06	4	0471040	5600620	190	Ilmenite norite	103.2	1.54	0.72	214	2	14	3	123	6	15	7	326	84	9	2
TL07	4	0470490	5600611	78	Norite	115.9	1.20	0.37	10	7	32	8	108	49	34	2	274	40	16	4
TL08	4	0470537	5600645	75	Ilmenitite	7.4	1.46	0.57	221	18	6	5	119	33	10	1	335	51	9	6
TL09	4	0470542	5600646	74	Deposit anorthosite	3.8	1.12	−0.05	192	13	23	15	283	6	44	20	40	76	44	12
TL10	4	0470591	5600669	76	Ilmenitite	7.9	1.68	0.68	55	0	18	6	145	35	13	2	325	55	14	2
TL11	4	0470811	5600574	81	Ilmenite norite	55.0	1.47	0.52	293	59	26	10	72	25	29	20	171	17	30	6
TL12	4	0470838	5600406	91	Ilmenitite	5.4	1.05	0.57	13	13	62	15	282	7	65	44	163	76	50	11
TL13	4	0470788	5600277	98	Ilmenite norite	21.9	1.66	0.86	222	16	40	14	59	73	40	6	313	5	14	6
TL14	4	0470705	5600209	98	Ilmenitite	31.9	2.59	0.74	47	23	9	0	300	35	9	5	164	46	6	1
TL15	4	0470489	5600502	86	Ilmenitite	14.5	1.48	0.24	52	29	32	9	149	12	24	7	259	58	22	9
TL16	4	0470422	5600565	89	Deposit anorthosite[a]	1.5	1.11	−0.23	344	9	31	9	84	48	52	31	246	41	54	5
TL17	4	0470375	5600677	98	Ilmenitite	5.3	1.29	0.98	199	10	57	2	107	13	57	3	327	74	3	1
TL18	4	0470434	5600769	98	Ilmenitite	91.3	3.55	0.91	108	33	25	2	227	38	25	3	351	35	3	2
TL19	4	0470938	5600744	202	Layered norite	23.1	1.18	0.50	36	16	45	7	303	11	41	19	180	71	25	17
TL20	4	0470944	5600815	212	Layered norite	11.8	1.10	0.45	58	22	48	27	258	66	44	30	151	7	36	25
TL21	5	0471244	5600495	250	Host anorthosite	0.82	1.09	0.31	355	26	26	10	261	7	29	6	157	63	17	7
TL22	4	0471208	5600387	254	Host anorthosite	0.93	1.13	0.10	41	30	15	2	286	36	15	5	160	39	10	5
TL23	5	0471026	5599896	247	Host anorthosite	0.78	1.11	−0.01	76	25	24	7	342	10	28	14	232	62	24	3
TL24	6	0471053	5600119	246	Host anorthosite	0.94	1.08	0.50	21	30	42	8	114	4	42	10	211	60	12	3
TL25	4	0470758	5599993	261	Host anorthosite	0.55	1.07	0.37	360	11	56	9	92	12	55	33	227	74	33	10
TL26	4	0470675	5600069	230	Host anorthosite[b]	0.35	1.16	−0.04	137	13	43	8	40	29	40	24	248	58	23	13
TL27	4	0470392	5600409	191	Ilmenitite	93.4	2.39	0.27	5	54	6	4	124	19	5	2	225	29	6	2
TL28	5	0470308	5600605	173	Ilmenitite	7.1	1.81	0.85	200	10	15	4	66	76	15	4	292	10	5	3
TL29	4	0470299	5600712	164	Ilmenite norite	29.4	1.37	−0.51	25	10	6	5	126	44	20	4	285	44	20	5
TL30	4	0470400	5600848	154	Ilmenitite	82.2	4.14	0.89	247	62	8	5	339	1	8	2	70	28	5	3
TL31	4	0470968	5601366	231	Host anorthosite	0.80	1.11	−0.26	226	6	16	2	133	29	16	11	327	60	11	3
TL32	4	0470366	5600486	183	Ilmenitite	17.5	2.60	0.84	18	63	15	1	128	10	15	2	223	25	2	1
TL33	4	0470512	5600525	75	Ilmenitite	49.6	2.01	0.76	67	1	11	5	164	81	16	6	337	9	17	1
TL34	5	0470929	5600316	135	Ilmenitite	5.3	1.17	0.81	4	12	60	13	96	8	60	10	222	76	14	12
TL35	4	0470920	5600310	135	Deposit anorthosite[b]	1.7	1.13	0.38	50	28	41	19	316	7	42	14	214	61	25	10
TL36	5	0470881	5600280	135	Layered norite	23.4	1.15	0.55	208	20	49	16	334	58	47	18	108	24	22	14
TL37	5	0470791	5600194	135	Deposit anorthosite	3.0	1.30	0.01	57	21	35	25	182	57	38	23	316	25	32	22
TL38	5	0470514	5600245	135	Ilmenitite	11.2	1.72	−0.33	41	22	9	2	152	42	12	3	291	40	13	5
TL39	4	0470614	5600170	135	Ilmenitite	46.0	1.69	0.21	63	29	9	7	313	32	16	1	185	44	15	9
TL40	4	0470748	5600395	88	Ilmenitite	48.9	2.05	0.68	305	18	38	16	187	55	61	13	46	29	62	14
TL41	4	0470630	5600857	185	Ilmenitite	19.0	2.44	0.84	203	10	14	4	105	39	13	8	305	49	11	8
TL42	4	0470062	5600405	317	Ilmenite norite	11.2	1.16	0.31	273	12	42	16	19	52	46	27	174	35	37	16
TL43	4	0469923	5600602	296	Ilmenitite	55.7	4.28	0.95	213	23	49	4	95	49	49	4	318	32	7	2
TL44	5	0470037	5600753	277	Ilmenitite	24.8	3.52	0.88	204	0	8	0	113	52	9	2	294	38	2	0
TL45	4	0470357	5600093	199	Ilmenitite	37.6	2.23	0.87	165	0	19	3	74	10	19	2	257	80	4	2
TL46	4	0470347	5600009	201	Ilmenitite	26.0	2.92	0.83	223	17	6	2	127	17	7	3	354	66	5	2

n: number of specimens; *X* and *Y*: coordinates (in m), in the NAD83 UTM grid (20 N zone); *Z*: altitude (in m); K_m: magnitude (in 10^{-3} SI) of the bulk magnetic susceptibility; P_j and T_j: anisotropy degree and shape parameter of Jelinek (1981); K_1, K_2 and K_3: long, intermediate and short principal axes of the AMS ellipsoid (K_1 is the magnetic lineation and K_3 the pole to the magnetic foliation); Dec and Inc: declination and inclination of the axes; σ_1 and σ_2: dimensions (in degrees) of the 2σ ellipse expressing the scattering of individual AMS measurements.

See e-Fig. 1 in Appendix A for equal-area projections of the individual AMS axes.

[a] Thick layer or lens, or shelf of wall-rocks.

[b] Leuconorite, according to the classification of Streckeisen (1974).

TL13, TL17 and TL43). They have different hemo-ilmenite, magnetite and sulfide contents, and various bulk magnetic susceptibility values (e-Table 1).

(Ilmenite) norites TL07 and TL13, that contain some primary and secondary magnetite, have M_s and M_{rs} values that both decay gradually with increasing temperature, until ca. 570 °C (Fig. 8a, b). The low-field susceptibility measurements for both samples indicate a Curie point slightly below 580 °C, at a slightly lower temperature than M_s (Fig. 8a, b), as would be expected (Fabian et al., 2013). The high-field susceptibility curves show a continued decay with increasing temperature (Fig. 8a, b), the curve for TL07 displaying a small, but sharp Hopkinson peak above 560 °C due to the magnetite, whereas for TL13 it is dominated by the paramagnetic behavior of the ilmenite component of hemo-ilmenite.

Ilmenitites TL17 and TL43 display dominantly concave downward curves for M_s and M_{rs}, and low-field susceptibility (Fig. 8c, d) showing a rapid decay close to ca. 600–605 °C, the approximate Néel temperature for the hemo-ilmenite (similar Néel temperatures, ca. 610–620 °C, have been reported by McEnroe et al., 2007 for nearly pure hemo-ilmenite samples from the Lac Tio ore body). The high-field susceptibility (Fig. 8c, d) is dominated in both samples by the paramagnetic contribution from the ilmenite. There is a small peak at ca. 180–220 °C in the low-field susceptibility curves (Fig. 8c, d), that we tentatively attribute to alteration products of the Fe–Ti oxides, as observed microscopically. For TL17, this small peak is roughly concordant with a slight decrease in the M_{rs} curve at ca. 200 °C and a "hump" in the M_s curve just below 200 °C. However, this "hump" could be due to a non-saturation effect. The magnetite lamellae observed in hemo-ilmenite

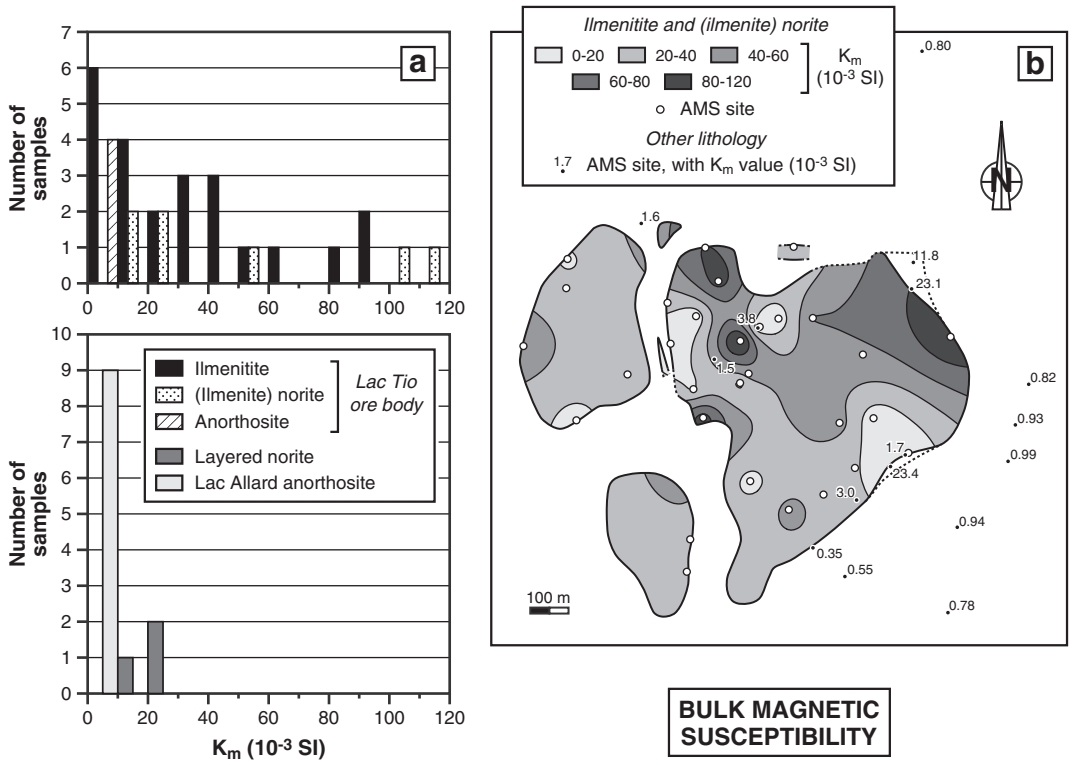

Fig. 9. (a) Partial histograms of the bulk magnetic susceptibility (K_m); (b) contoured map of K_m, established for ilmenitites and (ilmenite) norites only (the other lithologies are plotted with their own K_m value).

grains of sample TL43 (e-Table 1) likely contribute to the significant amount of M_s and M_{rs} which is lost at temperatures <550–560 °C (Fig. 8d).

To monitor for chemical change during the high-temperature experiments, room-temperature hysteresis measurements (not shown) were made before and after the high-temperature measurements. This hysteresis analysis showed little change in the magnetic mineralogy due to the heating, the loops being similar to these discussed above.

The thermomagnetic experiments, as the hysteresis results, demonstrate that the hemo-ilmenite and magnetite variably contribute to the magnetic properties of the Lac Tio ore body. The Curie temperatures, as measured on samples TL07 and TL13, further indicate that the magnetite is a Ti-poor titanomagnetite, near end member magnetite in composition. It is also worth noting that the thermomagnetic curves show no influence of pyrrhotite, even in sample TL07 that is relatively rich in various sulfides (ca. 2%, which is the highest sulfide content of the sample set). This must be related to the sporadic occurrence and usually trace amounts of this sulfide and/or implies that pyrrhotite in our samples is a non-ferromagnetic variety. It is thus reasonable to neglect the effect of pyrrhotite on the magnetic properties.

6. Anisotropy of low-field magnetic susceptibility

AMS describes the directional variability of magnetic susceptibility within a material, such as a rock. In a low-magnetic field, as a first approximation, AMS takes the form of a symmetrical second-rank tensor that can be represented geometrically by an ellipsoid. This ellipsoid, whose principal axes (labeled $K_1 \geq K_2 \geq K_3$) correspond to the eigenvectors of the AMS tensor, can be used to describe the magnetic fabric associated with the AMS. The arithmetic mean of the principal susceptibilities defines the bulk magnetic susceptibility [$K_m = (K_1 + K_2 + K_3)/3$]. The anisotropy degree and shape of the magnetic fabric (eccentricity and shape of the AMS ellipsoid) can be described by the P_j and T_j parameters of Jelinek (1981), respectively:

$$P_j = \exp\sqrt{2\sum_i (\ln K_i/K_m)^2}\,(i = 1 \text{ to } 3) \text{ and}$$

$$T_j = (2\ln K_2 - \ln K_1 - \ln K_3)/(\ln K_1 - \ln K_3).$$

The K_1K_2 plane, perpendicular to the K_3 axis, is referred to as the magnetic foliation and the K_1 axis is the magnetic lineation.

The AMS measurements have been performed on the 205 small cylinders cut from the cores drilled in the oriented samples. The AMS of each specimen was obtained, in a low magnetic field (300 A/m), using the Kappabridge KLY-3 susceptometer of AGICO Ltd. Measurements provided the length and orientation of the three principal axes of the AMS ellipsoid. For each oriented sample, an average ellipsoid was calculated from the AMS measurements made on the small cylinders, following the tensor averaging method of Hext (1963). The AMS data set is presented in Table 2 and in e-Fig. 1 (equal-area projections of the principal axes; Appendix A).

6.1. AMS scalar parameters

The bulk magnetic susceptibility (K_m), ranges over a large interval, from 0.35 to 115.9×10^{-3} SI (Table 2; see also Fig. 9a). Not surprisingly, the lowest values are observed in samples from the Lac Allard anorthosite ($\leq 1.6 \times 10^{-3}$ SI). Very similar, low susceptibility values are found in anorthosites from the Early-Neoproterozoic, ca. 0.93–0.92 Ga Rogaland anorthosite province of SW Norway (Diot et al., 2003; Brown and McEnroe, 2004, 2008). In ilmenitite (the dominant and, hence, most intensively sampled rock type in the ore body), K_m ranges from 5.3 to 93.4 $\times 10^{-3}$ SI. These values are consistent with susceptibility measurements made by Hargraves (1959) and McEnroe et al. (2007) on other

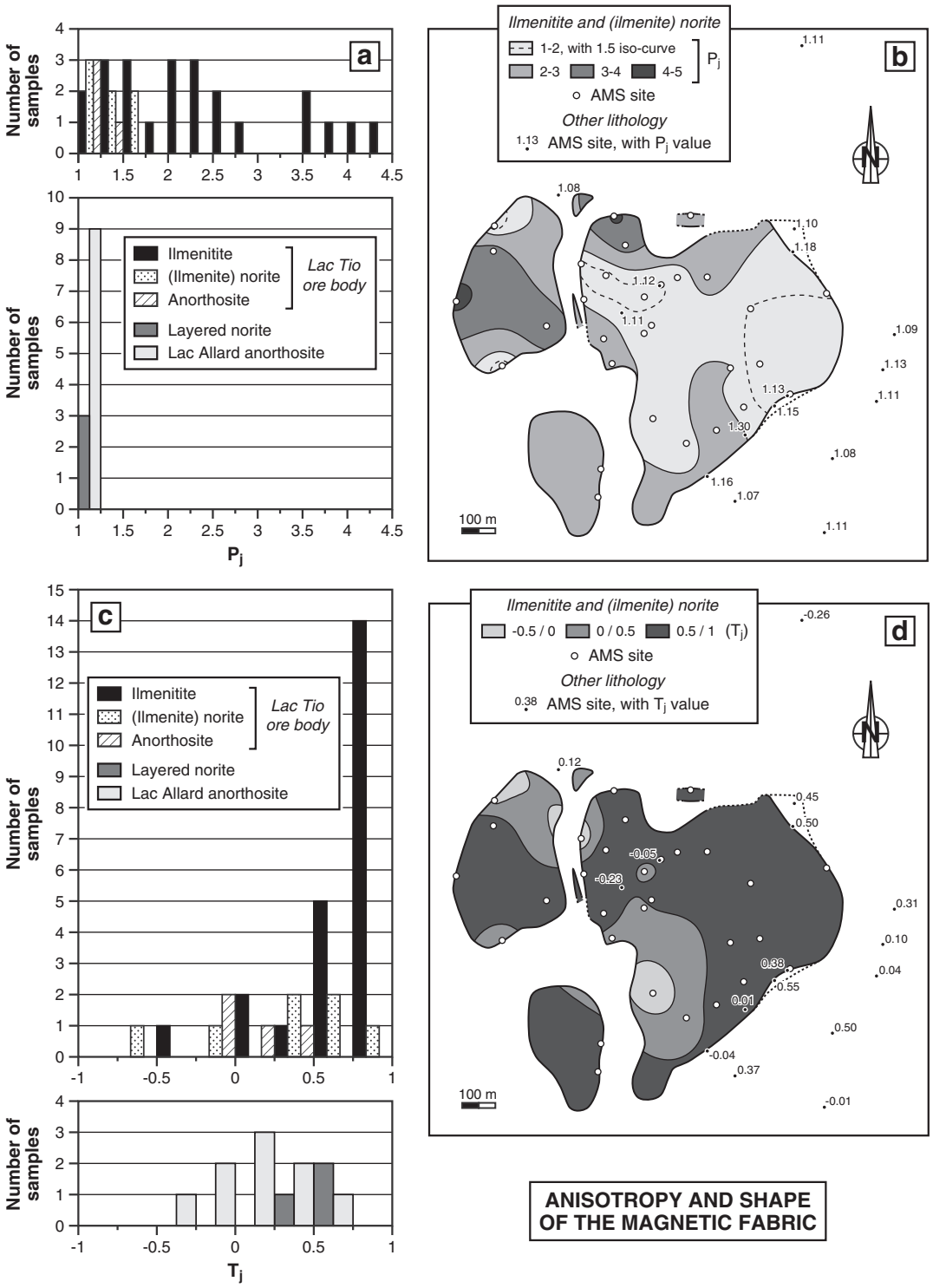

Fig. 10. (a) Partial histograms of the Jelinek's (1981) AMS anisotropy degree (P_j); (b) contoured map of P_j; (c) partial histograms of the Jelinek's (1981) AMS shape parameter (T_j); (d) contoured map of T_j. The contoured maps of Fig. 10b and d were established for ilmenitite and (ilmenite) norite samples only (the other lithologies are plotted with their own P_j or T_j value).

ilmenitites from the deposit (3.0–113.4 × 10^{-3} SI). An interpretation of the K_m values is presented below, rock type by rock type. It confirms and completes the conclusions of the hysteresis and thermomagnetic analyses concerning the mineralogical control on the magnetic properties.

By analogy with magnetic susceptibility thresholds established for more classical rock types worldwide (*e.g.* Bouchez, 2000; Rochette, 1987), the range of K_m values observed in the Lac Allard anorthosite (0.35–1.6 × 10^{-3} SI) indicates a contribution to the magnetic susceptibility ranging from dominantly paramagnetic to a mixed contribution of paramagnetic (Fe–Mg silicates, ilmenite component of ilmeno-hematite and hemo-ilmenite) and ferromagnetic minerals (hematite component and magnetite), with a negligible contribution of the diamagnetic

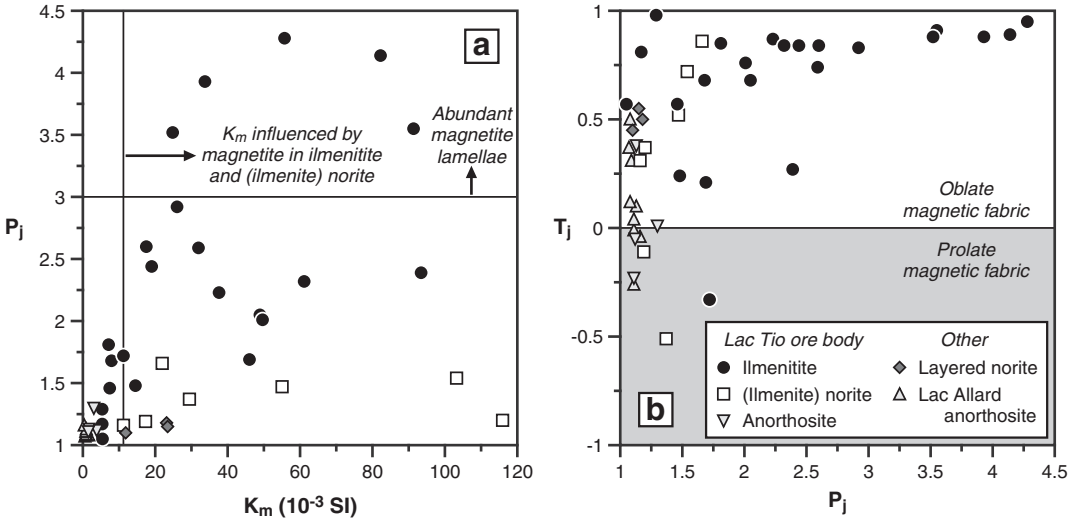

Fig. 11. (a) Plot of Jelinek's (1981) AMS anisotropy degree (P_j) *vs.* bulk magnetic susceptibility (K_m); (b) Jelinek's (1981) plot of AMS shape (T_j) *vs.* anisotropy degree (P_j). Symbols are the same for Fig. 11a and b (see caption in Fig. 11b).

minerals (plagioclase, excluding the oxide inclusions). K_m values in anorthosite from the ore body are, in average, slightly higher (1.5–3.8 × 10^{-3} SI), pointing to an increase of the ferromagnetic contribution.

In the other rock types, the K_m values are higher (>> 10^{-3} SI), indicating a dominantly ferromagnetic susceptibility. In ilmenitite samples containing no magnetite or negligible amount of this oxide, K_m ranges from 5.3 to 7.9 × 10^{-3} SI (e-Table 1) and the magnetic susceptibility is dominated by hemo-ilmenite, with a very strong control of the hematite component. In other ilmenitite samples, as well as in (ilmenite) norite and in layered norite, minor amounts of primary and/or secondary magnetite give higher K_m values (from 11.2 to 115.9 × 10^{-3} SI; e-Table 1). In these samples, magnetite exerts a more or less strong control on the magnetic susceptibility depending on its proportions, which explains (1) the great variability of K_m in ilmenitite (Fig. 9a), whereas variation in the hemo-ilmenite proportions from one sample to another (a few percents) is negligible in this rock type with regard to its average hemo-ilmenite content, and (2) the fact that ilmenitite and (ilmenite) norite display the same, highly variable K_m distribution (Fig. 9a), though they have distinct hemo-ilmenite contents. Even a small amount of magnetite easily overcomes the hematite signal because the intrinsic magnetic susceptibility of magnetite is up to ca. 400 times greater than that of hematite (Borradaile and Jackson, 2004; Dunlop and Özdemir, 2009; Rochette et al., 1992).

A contoured map of K_m, established for ilmenitite and (ilmenite) norite lithologies only exhibits small zones of maximum and minimum values that are heterogeneously distributed over the ore body (Fig. 9b). Small zones with K_m > 80 × 10^{-3} SI, as observed in the west of the main ore body and close to its eastern contact are defined by samples (TL30, TL18, TL07 and TL27, from north to south, in the west, and TL06 in the east; Fig. 2a) that have the highest magnetite content (ca. 2–2.5%, as calculated from the susceptibility values, following the simple approach of Robinson et al., 2013). This map illustrates the irregular distribution of the mineralogy, both at the scale of the ore body and at the outcrop scale.

The P_j parameter varies from 1.05 to 4.28 (Table 2; see also Fig. 10a). This large interval of values is actually that of the ilmenitite samples and indicates magnetic fabrics of highly variable strength for this rock type. The highest P_j values (>3), *i.e.* the strongest magnetic fabrics are observed in ilmenitite samples containing the greatest number of magnetite lamellae in hemo-ilmenite grains (TL03, TL18, TL30 and TL43-44; e-Table 1), which is in good agreement with the recent work of Robinson et al. (2013) suggesting that the shape anisotropy of these lamellae can play a role in the AMS of the Lac Tio hemo-ilmenite ore body. The other rock types sampled in the ore body have smaller and less variable anisotropy degrees (P_j from 1.16 to 1.66 in (ilmenite) norite, and from 1.11 to 1.30 in anorthosite). The Lac Allard anorthosite and the layered norite have weak magnetic fabrics of similar strength (P_j is 1.07–1.16 for the former and 1.10–1.18 for the latter). In a P_j *vs.* K_m diagram, there is no obvious correlation between P_j and K_m (Fig. 11a). However, three distinct "behaviors" are worth noting, *i.e.* weakly variable K_m and P_j values (anorthosite, layered norite), and highly variable K_m values coupled with either moderately (ilmenite norite and norite) or highly (ilmenitite) variable P_j values. A contoured map of P_j drawn for ilmenitite and (ilmenite) norite samples (Fig. 10b) exhibits two small zones of maximum values (P_j > 3) defined by ilmenitite samples with the highest amount of magnetite lamellae (TL03, TL18, TL30, TL43–44; e-Table 1; Fig. 2a). It shows also a large zone of lower anisotropy values (P_j < 2) that runs from the eastern to the western contact of the main ore body, along a roughly-defined, WNW–ESE direction. This zone of lower P_j values is independent of the rock type since it is defined both by ilmenitites and noritic samples. Therefore, the strength of the magnetic fabric is not fully controlled by the mineralogical composition: it is also correlated, at least locally, with the finite strain undergone by the ore body.

The T_j parameter ranges from −0.51 to 0.98, with negative values being observed in only 8 samples out of 46 (Table 2; see also Fig. 10c). The magnetic fabric is thus oblate in average, at the scale of the whole data set. In detail, neutral to moderately AMS ellipsoids are more frequent in anorthosite (T_j from −0.23 to 0.38 for the anorthosite deposit and from −0.26 to 0.50 for the host anorthosite) and layered norite (T_j = 0.45–0.55) than in ilmenitite and (ilmenite) norite where moderately to strongly oblate magnetic fabrics are dominating (T_j from −0.33 to 0.98 and −0.51 to 0.86, respectively). In a T_j *vs.* P_j plot (Fig. 11b), the most striking feature concerns the ilmenitite samples, that show a concentration in the uppermost part of the diagram, close to T_j = +1 (almost disk-shaped AMS ellipsoids) coupled with a scattering along the horizontal (P_j) axis (AMS ellipsoids with highly variable eccentricity). Contouring of T_j illustrates the dominant moderately to strongly oblate character of the magnetic fabric in ilmenitite and (ilmenite) norite (Fig. 10d). It also shows that the T_j negative values occur only at or close to the western flank of both the main ore body and the North-West deposit, pointing to a local strain effect on the shape of the AMS ellipsoid (shearing along the contact with the anorthosite wall rocks?).

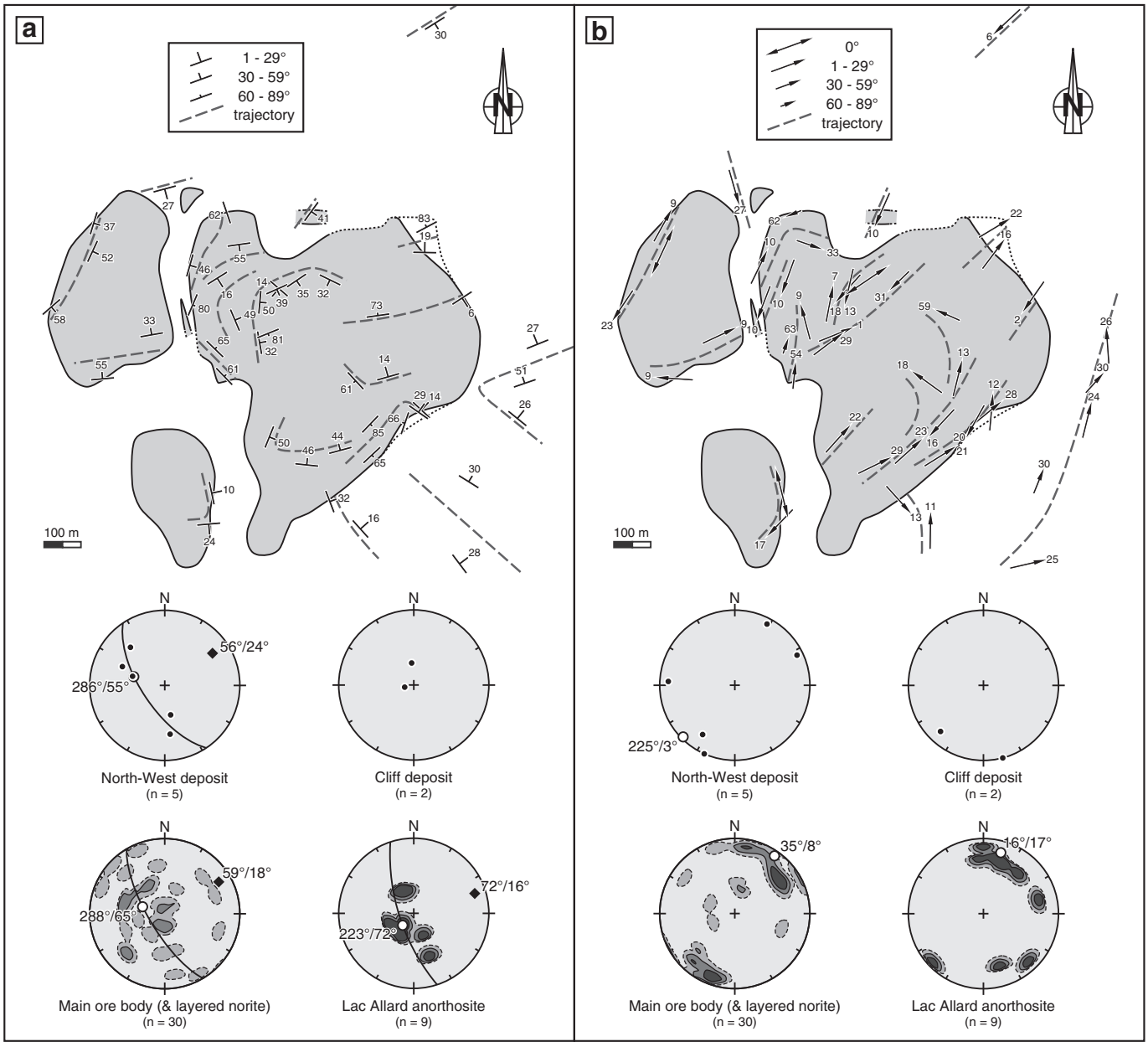

Fig. 12. Map of the magnetic (a) foliations and (b) lineations, with simplified trajectories and equal-area projections (lower hemispheres; contours at 1–3–6%; white dot: weighted average; arc of circle and gray diamond: cylindrical best fit and its pole).

6.2. AMS directional data

The orientation of the magnetic foliation is quite variable in the three portions of the Lac Tio ore body (Fig. 12a). However, a closer look at the data reveals that the trajectories of the magnetic foliation are usually parallel to the deposit margins, as seen in map view. Moreover, the dip of the magnetic foliation is usually consistent, both in direction and intensity, with the dip of the ore body walls that can be seen on the 3D reconstruction of Fig. 2b, c. It can thus be concluded that the pattern of the magnetic foliations mimics the 3D shape of the deposit. This suggests a close relationship between the orientation of the magnetic foliation and that of the igneous layering, even if such a relationship is not obvious when the layout of both planar structures is compared (such a comparison is made difficult by the scarcity of field measurements; Figs. 2 and 12a). Local perturbations in the pattern of the magnetic foliations, as observed *e.g.* in the central part of the main ore body (Fig. 12a), probably reflect upright folding, as evidenced in the field (Fig. 3a) and/or irregularities of the walls. Hargraves (1959) also found a close relationship between the magnetic foliations measured in boreholes drilled in the Lac Tio ore body and the orientation of the

Fig. 13. Equal-area projections (lower hemispheres) of hemo-ilmenite LPO obtained through EBSD measurements. For samples TL03 and TL38, EBSD data correspond to "test" measurements, made on thin sections cut parallel to the K_1K_3 AMS plane ($A=K_1$, $B=K_3$; see Table 2 for orientation of the AMS axes). For the other samples, EBSD measurements were conducted on vertical to subvertical thin sections ($A=0°/0°$, $B=0°/90°$ for TL06 and TL30; $A=0°/0°$, $B=270°/85°$ for TL10; $A=60°/10°$, $B=240°/80°$ for TL13). Density contours are in multiples of uniform distribution. They were carried out using the software PFch5 developed by D. Mainprice (http://www.gm.univ-montp2.fr/spip/spip.php?article576). *n*: number of measurements; *MD*: maximum of density; gray diamond: best axis. Projection of the AMS axes in the EBSD plane is shown, for the sake of comparison (square, K_1; triangle, K_2; circle, K_3), and the value of the angle between the best *c* axis and K_3 is given.

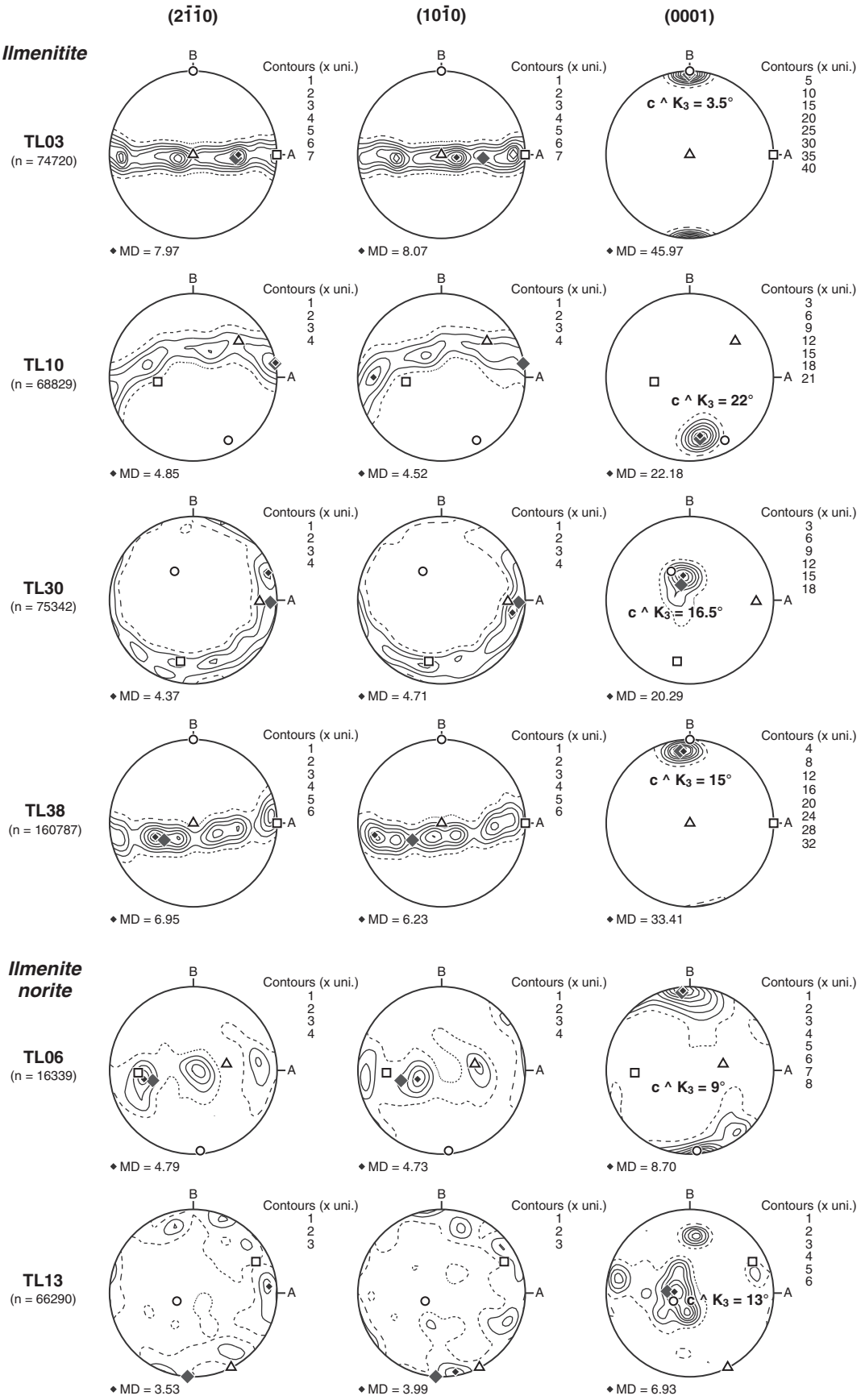
(2$\bar{1}\bar{1}$0)
(10$\bar{1}$0)
(0001)
Ilmenitite
TL03
(n = 74720)
TL10
(n = 68829)
TL30
(n = 75342)
TL38
(n = 160787)
Ilmenite norite
TL06
(n = 16339)
TL13
(n = 66290)
B
A
Contours (x uni.)
c ^ K3 = 3.5°
c ^ K3 = 22°
c ^ K3 = 16.5°
c ^ K3 = 15°
c ^ K3 = 9°
c ^ K3 = 13°
MD = 7.97
MD = 8.07
MD = 45.97
MD = 4.85
MD = 4.52
MD = 22.18
MD = 4.37
MD = 4.71
MD = 20.29
MD = 6.95
MD = 6.23
MD = 33.41
MD = 4.79
MD = 4.73
MD = 8.70
MD = 3.53
MD = 3.99
MD = 6.93

basal contact of the deposit, including wavy aspects of the foliation trend, as seen in cross section, above local irregularities of the floor.

In the basin-shaped North-West deposit, the magnetic foliations have a weighted average of N16°E/35°ESE and their poles in an equal-area projection define a partial girdle along a great circle, with a best-fit π-axis (or magnetic zone axis; Henry, 1997) of N56°E/24°NE (Fig. 12a). This axis can be taken as the axis around which the North-West deposit is (cylindrically) folded, at least as a first approximation since only five measurements are available. In the main ore body, the mean magnetic foliation is similar to that in the North-West deposit (N18°E/25°ESE, including measurements made in the layered norite; Fig. 12a), despite a much greater number of measurements, quite dispersed in the equal-area projection. The best-fit π-axis has also a similar orientation (N59°E/18°ENE), which suggests that the main ore body is also folded around a NE–SW- to ENE–WSW-striking, gently-plunging axis. For the Cliff deposit, only two measurements of magnetic foliations are available and the corresponding equal-area projection (Fig. 12a) is statistically meaningless.

In the Lac Allard anorthosite, the measured magnetic foliations have gentle to moderate dip values (between ca. 15° and 50°), and they are ENE–WSW-striking, with SSE or NNW dips, to the north and east of the ore body, and NW–SE-striking, with NE dips, to the south-west (Fig. 12a). Such an orientation complies with that of the S_0–S_1 structure, as measured in the field (Fig. 2). Therefore, the layout of the magnetic foliations on the map and the partial girdle defined by their poles on an equal-area projection (Fig. 12a) probably reflect (locally overturned) folding of the anorthosite in the vicinity of the Lac Tio ore body. The orientation of the fold axis, as given by the best-fit π-axis, is N72°E/16°ENE, which is similar to the best-fit π-axis found for both the main ore body and the North-West deposit. The mean magnetic foliation is N133°E/18°NE.

Compared to the magnetic foliation, the magnetic lineation displays a more regular pattern (Fig. 12b): most magnetic lineations are gently plunging, with a dominant NE–SW strike; magnetic lineations displaying moderate to steep plunge values (from 33° to 63°) and striking either parallel or at high angle to the gently plunging lineations are found only locally, mostly in the west of the main ore body. The two oblique, moderately to steeply plunging magnetic lineations that are observed at the NW corner of the main ore body correspond to two samples (TL18, TL30) that are relatively rich in lamellae of magnetite, and characterized by high K_m and P_j values (e-Table 1; Figs. 9b, 10b), pointing to a strong effect of these lamellae on the local disturbance of the magnetic lineation pattern.

The weighted average orientation of the magnetic lineations is N35°E/8°NE for the main ore body and N45°E/3°SW for the North-West deposit (Fig. 12b). These mean lineations are roughly parallel to the elongation of both portions of the Lac Tio ore body (ca. N20°E) and in good agreement with the best-fit π-axes determined for the magnetic foliation poles, with an angular departure in the range 25–30° (Fig. 12a). By analogy with magnetic fabric studies of synfolding granite plutons (Benn et al., 2001; Čečys and Benn, 2007; Pignotta and Benn, 1999), the latter relationship can be taken as a confirmation of the folding of the ore body. Orientation of the magnetic lineations in the Lac Allard anorthosite is strikingly similar to that in the ore body, with a mean value of N16°E/17°NNE (Fig. 12b).

7. Hemo-ilmenite LPO as a control of the AMS? EBSD contribution

On polished thin sections cut from ilmenitites and noritic samples, and oriented according to the AMS axes, it is found that the SPO of the hematite exsolution lamellae is consistent with the orientation of the K_1K_2 plane (Fig. 4f). Such a parallelism between crystallographically controlled exsolution lamellae and magnetic foliation, first documented by Hargraves (1959) in nearly pure hemo-ilmenite samples, suggests an AMS strongly influenced by a LPO of the hemo-ilmenite grains. Furthermore, Robinson et al. (2013) have developed recently a theoretical model, based on Fisher statistics, linking AMS (and natural remanent magnetization) to the LPO of hemo-ilmenite grains. This model was successfully tested through preliminary EBSD measurements made on two massive hemo-ilmenitite samples (one sample from the Lac Tio ore body and another one from a neighboring hemo-ilmenite deposit).

To confirm the hemo-ilmenite LPO in the Lac Tio ore body and to test its relationship with the AMS, we have performed EBSD measurements on hemo-ilmenite grains of six selected samples: four ilmenitites (TL03, TL10, TL30 and TL38) and two ilmenite norites (TL06 and TL13). In the EBSD technique, the primary beam of a scanning electron microscope is focused on a carefully polished sample section inclined at 70° with respect to the horizontal. These accelerated electrons undergo multiple diffractions on atomic layers inside the sample and the diffracted electrons can be detected on a fluorescent screen, where they form a typical pattern consisting of lines and bands called Kikuchi bands. This EBSD pattern is characteristic of the crystallographic structure and orientation of the sample region from which it originates, and provides, therefore, direct information on the crystallographic orientation (*e.g.* Prior et al., 1999).

All EBSD data were collected using the JEOL JSM 5600 of the Laboratoire Géosciences Montpellier, Université de Montpellier II (France). Typical working conditions of the scanning electron microscope were 17 kV for acceleration voltage, 50 mA for beam current and 40 mm for working distance. Recording and processing of the EBSD patterns were performed with the HKL CHANNEL 5 + software package. For all samples, the whole surface of the thin sections was investigated. Euler angles (φ_1, ϕ, φ_2 characterizing 3D orientation of crystal lattice (Bunge, 1982) were measured in automatic mode with sampling steps ranging from 35 to 80 μm depending on the mean grain size.

EBSD results are displayed on equal-area projections in Fig. 13. In these projections, the poles of the $2\bar{1}\bar{1}0$ and $10\bar{1}0$ prism planes form partial girdles along great circles, and the (0001) poles (*c*-axes) are clustered around a maximum value. These results demonstrate a LPO for the hemo-ilmenite grains, characterized by a strong preferred orientation of the basal (0001) plane of ilmenite along which hematite was exsolved. The hemo-ilmenite LPO is stronger in ilmenitites than in ilmenite norites. This is particularly marked for the (0001) poles, with a maximum density of 20.29–45.97 for the former rock type *vs*. 6.93–8.70 for the latter (Fig. 13). The EBSD analysis thus confirms the relationship between the SPO of the hematite exsolution lamellae and the hemo-ilmenite LPO, in particular, the preferred orientation of the (0001) plane.

Eigenvectors of the normalized orientation tensors describing the LPOs (Woodcock and Naylor, 1983) have been calculated from the EBSD data. Best axes deduced from this calculation (they correspond to the eigenvectors with the largest eigenvalue) are plotted on the equal-area projections of Fig. 13, together with the AMS axes that have been rotated to be projected on the LPO density diagrams. There is a good agreement between the orientation of the "best crystallographic" *c*-axes and the AMS K_3 axes ($c \wedge K_3 \leq 22°$), pointing to a close relationship between hemo-ilmenite LPO and magnetic fabric, since, at the scale of individual hemo-ilmenite grains, the intrinsic k_1k_2 plane is parallel to the basal (0001) plane, *i.e.* the intrinsic k_3 axis is parallel to the *c*-axis (Robinson et al., 2006, 2013; Uyeda et al., 1963). The smallest discrepancy between hemo-ilmenite LPO and AMS ($c \wedge K_3 = 3.5°$) is observed for sample TL03 that have the most clustered *c*-axis (maximum density of 45.97; Fig. 13) and the best defined K_3 axis (see the size of the 2σ confidence ellipse in Table 2), correlated with the strongest SPO of both the hematite exsolution lamellae and the rock-forming minerals (Fig. 4f). The angular departure between *c* and K_3 axes ranges from 9° to 22° for the other samples, and probably reflects greater analytical errors (*e.g.* less accurately cut sections).

The EBSD results demonstrate that the magnetic foliation (K_1K_2 plane) in ilmenitite and (ilmenite) norite samples from the Lac Tio ore body corresponds to the average orientation of the intrinsic k_1k_2 plane

of the hemo-ilmenite grains, *i.e.* a statistical layout of the hemo-ilmenite (0001) basal planes. We may also assume that the magnetic lineation (K_1 axis) in these rocks corresponds to the average orientation of the intrinsic k_1 axis of the hemo-ilmenite grains, *i.e.* a statistical layout of the k_1 axes lying in the hemo-ilmenite (0001) basal planes (zone axis). A similar relationship between magnetic fabric and LPO of hemo-ilmenite and ilmeno-hematite grains has been found by Bascou et al. (2002) in mylonitic granulites from the Ribeira Belt (SE Brazil) and by Kontny et al. (2012) in mylonitic garnet micaschists from the Seve Nappe Complex (Scandinavian Caledonides, Northern Sweden). In these rocks, the magnetic fabric and the LPO were shown to fit well with the petrofabric (mylonitic foliation and stretching lineation). The close relationship between AMS and hemo-ilmenite LPO, as evidenced here through the EBSD analysis, implies a strong influence of the hemo-ilmenite magneto-crystalline anisotropy on the magnetic fabric of ilmenitites and (ilmenite) norites.

Moreover, the observation that ilmenitite samples containing the greatest number of magnetite lamellae in hemo-ilmenite display very high P_j values (>3; e-Table 1) implies a control of the lamellae on the strength of the sample magnetic fabric, which indicates that a SPO of these oxide plates may influence the AMS, as previously suggested by Robinson et al. (2013). Given that the magnetite lamellae are parallel to the basal (0001) plane of the hemo-ilmenite grains, no modification in the magnetic fabric orientation has to be expected *a priori* from the contribution of these oxide plates. Accordingly, the magnetic fabric orientation of ilmenitite samples with the highest content in magnetite lamellae does not differ from that of neighboring AMS sites, with the notable exception of samples TL18 and TL30 whose magnetic lineation is highly discordant on the magnetic lineation pattern of the main ore body, as shown above (Fig. 12b). Actually, for both samples, the K_2 axis is more akin with the magnetic lineation of the neighboring sites (Table 2; Fig. 12b), suggesting an intermediate magnetic fabric (exchange between K_1 and K_2 axes; Ferré, 2002; Rochette et al., 1992) which could be due to the relative abundance of magnetite lamellae. It is worth noting that magnetic fabrics with very high degree of anisotropy ($P_j > 3$) have rarely been described in the literature, even in studies of highly deformed rocks. Such exceptionally high anisotropies have been evidenced for example in some ultramylonite samples studied by Kontny et al. (2012) and were interpreted to reflect an AMS dominated by the SPO of synkinematic, strained magnetites. In the Lac Tio ilmenitites, the magnetite lamellae whose SPO is responsible for very strong magnetic fabrics are not strain-related: they are growth features (Robinson et al., 2013) and the high anisotropy degrees they induce simply reflect their extreme shape anisotropy.

The other occurrences of magnetite (mostly secondary magnetite replacing Fe-sulfides and discrete primary magnetite grains, both interstitial to hemo-ilmenite), that dominates the magnetic susceptibility in a number of samples, could also influence the AMS, providing they display a SPO. The primary magnetite grains have a shape anisotropy (Fig. 5b) and are therefore very good candidates to be major contributors to the AMS, as it is also the case for secondary magnetite resulting from the more or less complete transformation of anisotropic sulfide grains (Fig. 5e). On the contrary, coronas and irregular areas of secondary magnetite likely have only a very weak influence on the AMS. The contribution to the AMS of anisotropic magnetite grains would be, moreover, concordant with the hemo-ilmenite LPO (*i.e.* flattening plane of the magnetite grains parallel to the statistical hemo-ilmenite (0001) plane and long axis of the magnetite grains parallel to the zone axis of the hemo-ilmenite (0001) planes). Indeed, on the maps of Fig. 12, there is no discrepancy in the magnetic fabric orientation between AMS sites where magnetite was not detected and AMS sites that contain magnetite. Also, amongst the samples analyzed by EBSD, ilmenite norite TL06, that is relatively rich in interstitial primary magnetite grains (e-Table 1), displays one of the best concordance between the c and K_3 axes ($c \wedge K_3 = 9°$).

The dominant moderately to strongly oblate character of the magnetic fabric in ilmenitite and (ilmenite) norite, evidenced above through the interpretation of the T_j values, is now easy to explain: (1) the dominant oblate character indicates that the magnetic foliation (parallel to both the statistical basal (0001) plane of hemo-ilmenite and flattening plane of interstitial magnetite) is usually best defined than the magnetic lineation (parallel to both the zone axis of the hemo-ilmenite basal (0001) planes and the statistical long axis of the interstitial magnetite) and (2) the magnitude of the oblateness (T_j values commonly close to +1) has to be related to the platy habit of the hematite and magnetite lamellae that underlines the hemo-ilmenite (0001) planes.

For the rock types not analyzed by EBSD, *i.e.* the host and deposit anorthosite, and the layered norite, we may assume that the AMS also results from a LPO of hemo-ilmenite grains (and/or ilmeno-hematite in anorthosite) that combines with a SPO of magnetite (discrete grains, plus lamellae in hemo-ilmenite for the layered norite). A significant contribution from a LPO of paramagnetic silicates has also to be considered for the anorthosite samples.

In short, AMS in the Lac Tio ore body is dominated by a LPO of hemo-ilmenite grains and a concordant SPO of magnetite lamellae and interstitial grains. Most probably, there is a growing influence of the latter with increasing values of the bulk magnetic susceptibility (increasing magnetite content), the magnetite SPO being dominant in the high-susceptibility samples. The hemo-ilmenite LPO (and the magnetite lamellae SPO that mimics this LPO) and the SPO of the discrete magnetite grains were probably acquired continuously, from the emplacement and crystallization of the deposit to sub-solidus conditions, with solid-state deformation together with dynamic recrystallization, as attested by the microscope observations, operating in continuity with the magmatic deformation. They have not been destroyed by the subsequent static recrystallization. Preservation of a LPO by static recrystallization is a common feature, contrary to SPO which can be destroyed by this process because it strongly modifies the geometry of grain boundaries (*e.g.* Passchier and Trouw, 2005). The static recrystallization could even have reinforced the existing hemo-ilmenite LPO, through the disappearing of misoriented grains for the benefit of grains with a better orientation. It is also worth to note that thermal gradient responsible for static recrystallization is a potential mechanism of AMS development in igneous rocks, as suggested experimentally by Huang et al. (2009). In the present case, however, the LPO and SPO, and the associated magnetic fabric were acquired before the static recrystallization, as discussed above, and the role of the thermal gradient as a source for the AMS can thus be ruled out.

8. AMS as a proxy of the rock shape fabric? Image analysis contribution

To verify the coaxiality between magnetic fabric and petrofabric, we have conducted an image analysis on a selection of seven samples, *i.e.* most samples already investigated by EBSD (ilmenitites TL03, TL10, TL30, and ilmenite norites TL06, TL13), plus one layered norite (TL36) and one sample from the Lac Allard anorthosite (TL23). The principle of such a technique is to quantify the shape fabric or SPO of a given population of grains in a sample, through the treatment of digitized images of several, differently oriented sections.

For the image analysis, we have chosen the intercept method of Launeau and Robin (1996, 2005), which is based on an analysis of the boundary orientation distribution of objects. Using this method, quantification of the shape fabric was first conducted, for each selected sample, on scanned images of three mutually orthogonal sections (these images had been first carefully redrawn using a drawing software for the darkest samples, *i.e.* all samples except TL23 and TL36; Fig. 14a). The output of this 2D analysis is the aspect ratio (ellipticity) and the orientation of the principal axes of an ellipse describing the shape fabric in the sections (Fig. 14a). These orthogonal 2D data were then used to reconstruct an ellipsoid representative of the shape fabric of the sample

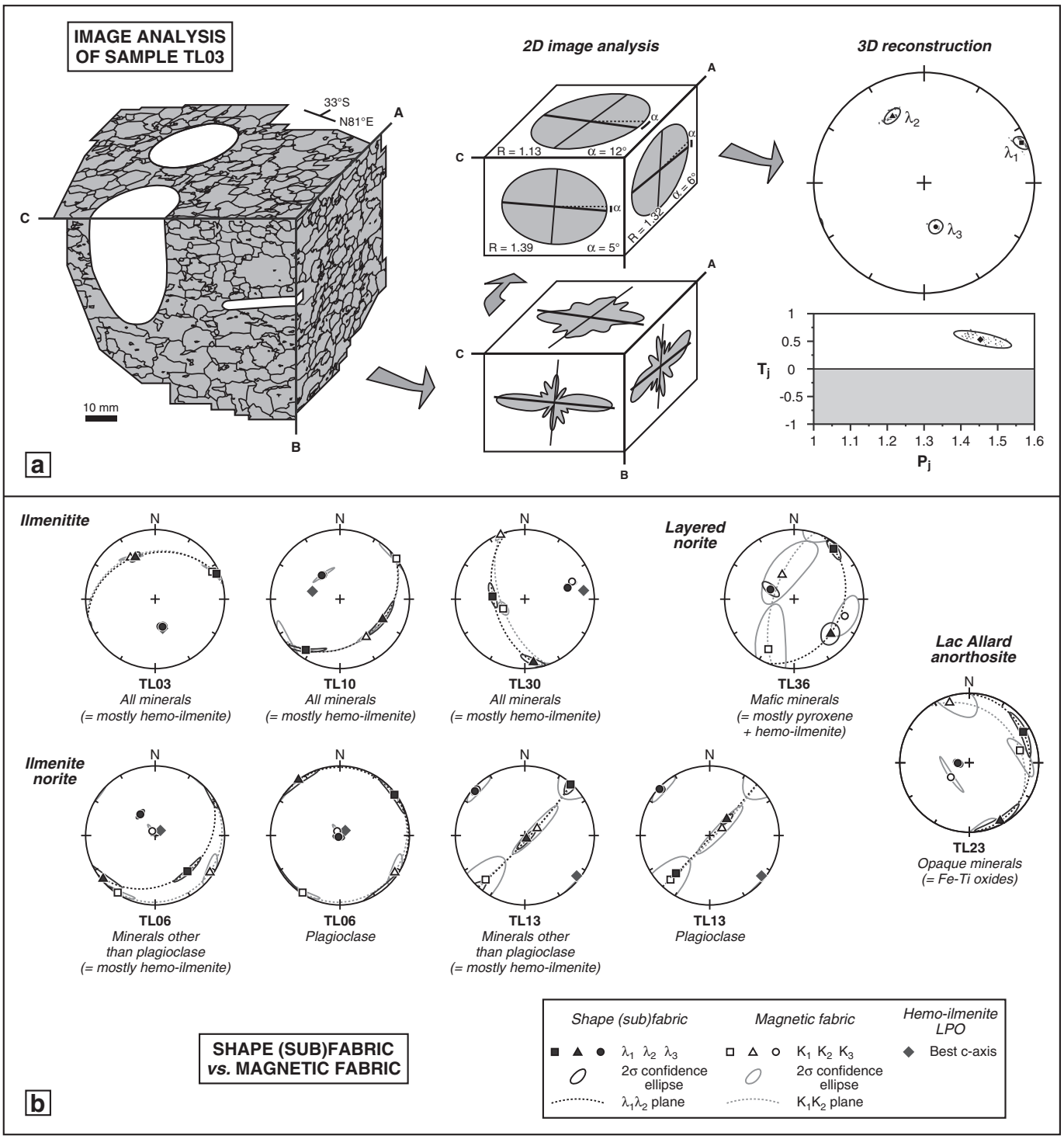

Fig. 14. (a) Image analysis procedure, as illustrated for ilmenitite sample TL03 — from left to right, (1) grain boundaries drawn from scanned images of three mutually orthogonal sections cut in the sample (the orientation of the upper section is indicated; white areas are holes and grooves, after drilling and sawing of the sample), (2) intercept roses and equivalent shape ellipses with aspect ratios and orientation of the long axes, determined for each section using the intercept method of Launeau and Robin (1996, 2005), and (3) characteristics of the shape ellipsoid, as reconstructed from the 2D analysis (projection of the long, intermediate and short axes of the ellipsoid (λ_1, λ_2, λ_3) on an equal-area diagram, lower hemisphere; Jelinek's (1981) plot of shape (T_j) *vs.* anisotropy degree (P_j); small gray dots, ellipses and black symbols are raw data, 2σ confidence ellipses and average values, respectively). (b) Equal-area projections (lower hemispheres) of the principal axes of shape (sub)fabrics (λ_1, λ_2, λ_3) obtained through image analysis (projections of the principal axes of the magnetic fabrics and the best *c*-axes of the hemo-ilmenite fabrics are also shown, for the sake of comparison).

(Fig. 14a). For ilmenitites (TL03, TL10, TL30), the analysis was conducted on all minerals and the shape fabric is thus an overall fabric. This fabric is, however, largely dominated by hemo-ilmenite that makes up more than 95% of the sample. For ilmenite norites (TL06 and TL13), two subfabrics were quantified: the subfabric of plagioclase grains and aggregates, and the subfabric defined by the other minerals (largely dominated by hemo-ilmenite). The image analysis technique was applied to the mafic minerals (mostly orthopyroxene and hemo-ilmenite) for the layered norite TL36 and to the opaque minerals (mostly hemo-ilmenite and ilmeno-hematite) for the host anorthosite TL23.

Table 3 gives the declinations and inclinations of the principal axes of the shape (sub)fabric (here called "shape axes") established through

Table 3
Image analysis data (and comparison with AMS data).

Rock type	Sample		A	B	C	P_j	T_j
Ilmenitite	TL03	IA[a]	68/5	335/34	165/56	1.45	0.53
		AMS	64/9	329/31	169/57	3.93	0.88
		Δ	6	6	2	2.48	0.35
	TL10	IA[a]	214/13	116/32	322/55	1.28	0.51
		AMS	55/0	145/35	325/55	1.68	0.68
		Δ	25[b]	24	2	0.40	0.17
	TL30	IA[a]	274/52	172/9	75/37	1.33	0.40
		AMS	247/62	339/1	70/28	4.14	0.89
		Δ	17	16[b]	10	2.81	0.49
Ilmenite norite	TL06	IA[c]	138/30	230/3	325/59	1.44	0.45
		AMS	214/2	123/6	326/84	1.54	0.72
		Δ	77	74	25	0.10	0.27
		IA[d]	54/2	323/1	221/88	1.67	0.37
		AMS	214/2	123/6	326/84	1.54	0.72
		Δ	21[b]	21[b]	7	0.13	0.35
	TL13	IA[c]	42/2	150/85	312/5	1.35	0.55
		AMS	222/16	59/73	313/5	1.66	0.86
		Δ	18[b]	18	1	0.31	0.31
		IA[d]	221/28	47/62	313/2	1.74	0.34
		AMS	222/16	59/73	313/5	1.66	0.86
		Δ	12	12	3	0.08	0.52
Layered norite	TL36	IA[e]	39/9	133/28	293/60	1.24	−0.25
		AMS	208/20	334/58	108/24	1.15	0.55
		Δ	31[b]	88	84	0.09	0.80
Host anorthosite	TL23	IA[f]	61/12	152/6	267/77	1.20	0.65
		AMS	76/25	342/10	232/62	1.11	−0.01
		Δ	19	19[b]	19	0.09	0.66

A, *B*, *C*, P_j, T_j: orientation (declination/inclination) of the long (*A*), intermediate (*B*) and short (*C*) principal axes, and anisotropy degree (P_j) and shape parameter (T_j) of Jelinek (1981), for the shape (sub)fabric defined through image analysis (IA) and for the magnetic fabric (AMS), with difference (absolute value) between IA and AMS data (Δ).
[a] All minerals (mostly hemo-ilmenite).
[b] Axes plunging in opposite directions.
[c] Minerals other than plagioclase (mostly hemo-ilmenite).
[d] Plagioclase.
[e] Mafic minerals (mostly pyroxene + hemo-ilmenite).
[f] Opaque minerals (Fe–Ti oxides).

image analysis for the seven samples. It lists also the values of the P_j and T_j parameters (Jelinek, 1981) calculated to express, respectively, the anisotropy degree and shape of the (sub)fabric. Fig. 14b displays equal area diagrams with projections of the shape axes. A comparison with the AMS data is made in Table 3 and Fig. 14b. The best *c*-axes of the hemo-ilmenite grains, determined through the EBSD analysis, are also shown in Fig. 14b.

Fig. 14b shows that the shape axes are usually well clustered. For the ilmenitite and ilmenite norite samples, these axes are usually close to the AMS axes, both for the hemo-ilmenite dominated (sub)fabric and the plagioclase subfabric (angular deviation ≤10° for the short axis, and ≤25° for the long and intermediate axes; Fig. 14b; Table 3). The only noticeable exception concerns ilmenite norite TL06 (Fig. 14b; Table 3): for this sample, the hemo-ilmenite dominated subfabric does not fit the magnetic fabric, the angular deviation being rather small for the short axis (25°), but very high for the long and intermediate axes (ca. 75°), while the shape axes of the plagioclase subfabric correlate well with the AMS axes. This situation expresses a slight obliquity between the SPO of hemo-ilmenite and plagioclase grains that is observed on the analyzed sections of the sample. We are confronted here with a peculiar case, where the recrystallization of the hemo-ilmenite could have not only destroyed, but also modified the primary SPO of the grains. The overall conformity of the hemo-ilmenite best *c*-axes, subparallel to the K_3 axes, with the short shape axes in ilmenitites and ilmenite norites (Fig. 14b) shows further that the statistical basal (0001) plane of hemo-ilmenite, subparallel to the magnetic foliation, corresponds to the flattening plane of the rock-forming minerals, mostly hemo-ilmenite and plagioclase, that underlines the igneous layering. The opaque subfabric in sample TL23 (host anorthosite) is also almost coaxial with the magnetic fabric (angular deviation for the principal axes <20°; Fig. 14b; Table 3), in agreement with the concordant attitude of the magnetic foliation and the S_0–S_1 structure, as evidenced above for the Lac Allard anorthosite. For sample TL36 (layered norite), there is a strong discrepancy between the shape axes of the mafic minerals and the AMS axes, with a moderate angular deviation for the long axis (31°), but an inversion between the short and intermediate axes (Fig. 14b; Table 3). Such a discrepancy suggests either an abnormal magnetic fabric (Ferré, 2002; Rochette et al., 1992) or an AMS linked to an ill-defined, secondary petrofabric.

The image analysis thus demonstrates that the magnetic fabric is coaxial with the rock shape fabric, with a few exceptions. This means that the AMS can be used as a proxy for the orientation of the petrofabric, at least on a statistical point of view (*i.e.* disregarding some abnormal orientations). In particular, the magnetic foliation proxies for the igneous layering in the ore body and for the S_0–S_1 structure in the host anorthosite. The magnetic lineation also reveals a linear arrangement of the rock-forming minerals that is hardly detectable through direct observation, most probably a mineral lineation that approximates the axis of maximum finite stretching. The orientation of this lineation is similar in the ore body and the Lac Allard anorthosite (NE–SW to NNE–SSW strike and gentle plunge, in average), as demonstrated by the concordance between the magnetic lineations inside and outside the ore body (Fig. 12b). Finally, the coaxiality between magnetic fabric and rock shape fabric definitely confirms that the layout of the magnetic fabric in the Lac Tio ore body expresses folding of the deposit around a NE–SW to ENE–WSW-striking, gently-plunging axis (Fig. 12).

Values of the P_j parameter calculated from the image analysis data for ilmenitites and ilmenite norites (Table 3) indicate shape subfabrics that are less anisotropic than the magnetic fabrics for hemo-ilmenite (lower P_j values), whereas they are slightly more anisotropic for plagioclase (slightly higher P_j values). The strong shape anisotropy of many plagioclase grains in ilmenite norites (Fig. 4b) explains this observation. When the T_j values are considered (Table 3), it appears that all shape subfabrics are oblate for the ilmenitites and ilmenite norites, as the corresponding magnetic fabrics, but with a less marked flattening (lower positive T_j values). This is another indication of the major role played by platy objects (hematite exsolutions and magnetite lamellae) in defining the AMS. It is also worth noting that the shape subfabric in ilmenite norites is slightly more flattened (slightly higher positive T_j values) for hemo-ilmenite than for plagioclase, which witnesses again differences in the morphology of the two minerals. For the layered norite TL36 and the host anorthosite TL23, the shape subfabric of the mafic minerals is slightly more anisotropic than the magnetic fabric, and the shape parameters are completely different (Table 3).

The image analysis confirms that the anisotropy degree and the shape parameter of the magnetic fabric are not necessarily, simply related to, respectively, the strength and the degree of flattening or stretching of the petrofabric, as it is commonly the case (*e.g.* Borradaile and Jackson, 2004; Rochette et al., 1992). The present study thus confirms that image analysis is an efficient and complementary tool providing useful data for interpretation of fabrics in igneous bodies (Plissart et al., 2012).

9. Geological implications

9.1. The Lac Tio ore body: A probable sag point at the margin of a ballooning anorthosite diapir

We have interpreted above the common boudinage of anorthosite layers (Fig. 3a, b) and the local occurrence of meter-scale isoclinal slump folds observed in the open pit as indicating a syn-emplacement, gravitational subsidence of the Lac Tio ore body. The shape of the deposit (Fig. 2b, c), as well as its internal structure outlined by the layout of the magnetic fabric (Fig. 12) are hardly reconcilable with such a simple gravitational process that would have produced lineations plunging

towards the thickest part of the ore body (*e.g.* Bolle et al., 2002; McBirney and Nicolas, 1997), *i.e.* to the east, whereas the observed stretching direction is ca. NE–SW. Actually, the AMS data indicate that the Lac Tio hemo-ilmenite ore body was strained, together with its anorthosite wall rocks, during a deformation event combining extension along a subhorizontal, ca. NE–SW direction and contraction in the perpendicular direction (see orientation of the magnetic lineation and axis of the folded magnetic foliation). This deformation probably occurred in the continuity of the gravitational deformation and has partly erased its effects. The decametric-scale upright folds locally observed in the ore body (Fig. 3a) may be interpreted as parasitic folds on the large-scale folds produced during this event. It is difficult to distinguish between the two deformation events in the role they played in the intracrystalline deformation and dynamic recrystallization of the deposit rock-forming minerals.

According to Gobeil et al. (2003) and Rivers (2012), the deformation of the Havre-Saint-Pierre anorthosite suite and that of the Saint-Jean domain as a whole has been dominated by the Grenvillian (Ottawan) NW-directed thrusting. Evidence of such a thrusting are numerous in the NW, strongly deformed portion of the Havre-Saint-Pierre anorthosite suite, in the vicinity of the 51st Parallel deformation corridor (Gobeil et al., 2003). NW thrust movements also occurred along the Romaine and Abbé-Huard shear zones (Madore et al., 1999; Verpaelst et al., 1999), prior to sinistral strike–slip and normal reworking (Indares and Martignole, 1993). This oblique reworking is characterized by ESE-plunging lineations, along which a downward displacement of the Natashquan domain relative to the Saint-Jean domain occurred. It would have been coeval with tectonic juxtaposition of the two domains, and of the a*MP* Belt and a*LP* Belt at the scale of the Grenville province, during late-Ottawan orogenic collapse, according to Rivers (2012).

The dome-shaped structure, and the internal deformation and dynamic recrystallization of the Lac Allard anorthosite and neighboring anorthosite bodies, as well as formation of tight synforms and high-strain zones in the mangeritic envelopes separating these bodies have also been attributed to regional contraction associated with the Ottawan NW-directed thrusting (Gobeil et al., 2003; Rivers, 2012). Alternatively, accepting a model of diapiric emplacement for the Havre-Saint-Pierre anorthosites, in agreement with the consensus petrogenetic model of the Proterozoic anorthosites (Ashwal, 1993), the morphology, deformation and dynamic recrystallization of the anorthosite domes might be interpreted in terms of syn-emplacement deformation due to the anorthosite buoyancy, which does not preclude any coeval tectonic shortening (Dobmeier, 2006). Furthermore, it appears that the structural interpretation of the Havre-Saint-Pierre anorthosite suite provided by Gobeil et al. (2003) and Rivers (2012) has to be adapted, in order to take into account the occurrence of the two magmatic pulses revealed by the geochronological data (Emslie and Hunt, 1990; Morisset et al., 2009; van Breemen and Higgins, 1993; Wodicka et al., 2003). Hence, it is obvious that the portions of the Havre-Saint-Pierre anorthosite suite belonging to the ca. 1.13 Ga pre-Grenvillian magmatic pulse have been affected by the NW-directed Ottawan thrusting (this probably applies *e.g.* to the portion of the Havre-Saint-Pierre anorthosite suite close to the 51st Parallel deformation corridor), whereas intrusions such as the Lac Allard anorthosite that were emplaced during the ca. 1.06 Ga magmatic event, *i.e.* following or near the end of the Ottawan metamorphic peak, have been less affected or possibly escaped the effects of the Ottawan deformation. This agrees with the tectonomagmatic models proposed by Corrigan and Hanmer (1997), and McLelland et al. (2010) for the emplacement of AMCG complexes in the Grenvillian orogen, according to which the Lac Allard anorthosite and the other ca. 1.06 Ga of the Havre-Saint-Pierre anorthosite suite would have been associated with late-orogenic collapse and extension, following the Ottawan crustal thickening.

The ca. NE–SW stretching direction evidenced in the present study, in the Lac Tio ore body and its anorthosite wall rocks is striking roughly parallel to the eastern border of the Lac Allard anorthosite that is outlined by an elongated mangeritic rim and the Romaine shear zone (Fig. 1). Such an orientation cannot be related to the NW-directed Ottawan thrusting (Gobeil et al., 2003; Rivers, 2012), or with the transtension event responsible for the oblique reworking of the Abbé-Huard shear zone and characterized by ESE-plunging lineations (Indares and Martignole, 1993). The gently-plunging extension direction, roughly parallel to the border of the Lac Allard anorthosite and coupled with contraction in the perpendicular direction would be more in agreement with ballooning of the anorthosite, *i.e.* a radial expansion of the igneous body, causing flattening and subhorizontal stretching of its external portion (Paterson and Vernon, 1995). The straining of the Lac Tio ore body in the outer portion of the Lac Allard anorthosite is therefore attributed to a ballooning process, that would be related to the final stage of diapiric emplacement of the enclosing anorthosite. The intensity of such a ballooning would have been rather limited, given the small degree of flattening associated with the contraction. Closure temperatures calculated by Morisset et al. (2009) for zircons from the Lac Allard anorthosite (ca. 940 °C) provide a climax temperature for the straining environment. More structural data on the Lac Allard anorthosite are, of course, required to constrain the deformation model that is proposed here.

9.2. Comparison with the Grader layered intrusion

A valuable comparison between the structure and strain history of the Lac Tio ore body, and those of the Grader layered intrusion can be made. The Grader intrusion (Charlier et al., 2008) crops out in the Lac Allard anorthosite, at ca. 4 km to the south-west of the Lac Tio ore body (at the scale of Fig. 1, this intrusion is hardly distinguishable from the Lac Tio ore body and it is therefore not located on the figure). It is a small igneous body (2400 m × 300–1000 m, as seen in map view), dominantly made up of layered (gabbro)norite, nelsonite and massive hemo-ilmenite (ilmenitite). The latter rock type, together with minor anorthosite, forms a small unit at the base of the intrusion (the Grader deposit) that was mined in the late 1940s.

The Grader intrusion has a basin-like structure, for which we have determined an axis of N16°E/30°SSW (best-fit π-axis for the distribution, in an equal-area projection, of 72 layering poles; 18 measurements from layered (gabbro)norite and nelsonite; Charlier et al., 2008; and 54 measurements from the Grader deposit; K. Stanaway, pers. comm. 2012). Such an orientation is relatively close to both the fold axis of the Lac Tio ore body and the average stretching direction, as determined in the present study (Fig. 12). The Grader deposit also shows structural similarities with the Lac Tio ore body, at the outcrop scale (K. Stanaway, pers. comm. 2012): (1) anorthosite layers are commonly stretched, forming angular boudins in the ilmenitite, (2) meter-scale isoclinal slump folds are prominent and (3) relatively open folds (with axes plunging ca. 30°S, *i.e.* subparallel to the here determined axis of the Grader intrusion) are observed locally. The Grader intrusion, as the Lac Tio ore body, has thus been affected by a collapse phenomenon due to a high density contrast with the anorthosite wall rocks, and by an event of folding (around a NNE–SSW axis) that we attribute to ballooning of the enclosing anorthosite and which is responsible for both the basin-like structure of the intrusion and outcrop-scale relatively open folds.

10. Conclusions

Microscope observations, room-temperature hysteresis measurements, thermomagnetic experiments and investigation of the bulk magnetic susceptibility reveal that the magnetic mineralogy of ilmenitites and (ilmenite) norites from the Lac Tio ore body is dominantly ferromagnetic, with a mixed contribution of hemo-ilmenite grains and magnetite of various origins (reduction–exsolution lamellae in hemo-ilmenite, discrete primary grains and secondary magnetite replacing Fe-sulfides). In anorthosite layers and lenses distributed in the ore

body, as well as in the surrounding Lac Allard anorthosite, there is an additional, important paramagnetic contribution (ilmenite component of ilmeno-hematite and hemo-ilmenite, ortho- and clinopyroxenes, hornblende, biotite).

EBSD data show that the hemo-ilmenite grains of the ore have a LPO characterized by a strong preferred orientation of the basal (0001) plane of ilmenite along which hematite was exsolved. This preferred orientation is subparallel to the magnetic foliation, which points to a close relationship between hemo-ilmenite LPO and AMS, thus implying a strong influence of the hemo-ilmenite magneto-crystalline anisotropy on the magnetic fabric. A SPO of the magnetite, especially the magnetite lamellae found in hemo-ilmenite, that exert a strong control on the magnetic fabric strength in some samples, may enhance and even overcome the hemo-ilmenite magneto-crystalline anisotropy. 3D image analysis demonstrates that the magnetic fabric is coaxial with the rock shape fabric, both in the ore body and the host anorthosite. Hence, the magnetic foliation proxies for the igneous layering in the former and for the S_0–S_1 structure in the latter, and the magnetic lineation proxies for an ill-defined mineral lineation that approximates the axis of maximum finite stretching.

The magnetic foliation in the ore body is distributed (folded) around a NE–SW- to ENE–WSW-striking, gently-plunging axis. This axis is close to the average magnetic lineation that has a similar orientation in the ore body and the anorthosite wall rocks (NE–SW to NNE–SSW strike and gentle plunge). Interpretation of this layout, in the light of the EBSD and image analysis data, indicates that the Lac Tio ore body was strained, together with the host anorthosite, during a deformation event combining extension along a subhorizontal, ca. NE–SW direction and contraction in the perpendicular direction. A ballooning process, related to the final stage of diapiric emplacement of the Lac Allard anorthosite, would be responsible for that deformation which probably occurred in the continuity of a syn-emplacement, gravitational subsidence of the heavy ore body into the lower density host anorthosite. Evidence for such a gravitational deformation is the common boudinage of anorthosite layers and the local occurrence of meter-scale isoclinal slump folds. The deformation model that is proposed here is also suitable to explain the structure and strain history of the neighboring Grader layered intrusion.

The location of both the Lac Tio ore body and the Grader layered intrusion at the margin of the Lac Allard anorthosite is probably not incidental. It possibly reflects collection of the Fe–Ti-rich (Charlier et al., 2008, 2010) and, therefore, high-density parent magmas by draining through the anorthosite crystal mush, along sloping floors of the rising diapir (Vander Auwera et al., 2006).

Acknowledgments

Rio Tinto is gratefully acknowledged for the financial support and permission to publish the data. K. Stanaway kindly provided unpublished data on the Grader layered intrusion. K. Svendby helped with the hysteresis and thermomagnetic measurements, and K. Fabian processed the high temperature magnetic data. C. Guilbaud, J.-P. Cullus and S. Malpas are thanked for the preparation of the polished thin sections. Constructive reviews by E.C. Ferré and an anonymous reviewer helped to strengthen the final version of the manuscript.

Appendix A. Supplementary data

Supplementary data associated with this article (e-Table 1 and e-Fig. 1) can be found, in the online version, at http://dx.doi.org/10.1016/j.tecto.2014.01.012.

References

Ashwal, L.D., 1993. Anorthosites. Springer-Verlag, Heidelberg (422 pp.).
Bascou, J., Raposo, M.I.B., Vauchez, A., Egydio-Silva, M., 2002. Titanohematite lattice-preferred orientation and magnetic anisotropy in high-temperature mylonites. Earth Planet. Sci. Lett. 198, 77–92.
Benn, K., Paterson, S.R., Lund, S.P., Pignotta, G.S., Kruse, S., 2001. Magmatic fabrics in batholiths as markers of regional strains and plate kinematics: example of the Cretaceous Mt. Stuart Batholith. Phys. Chem. Earth 26, 343–354.
Bergeron, M.B., 1986. Minéralogie et géochimie de la suite anorthositique de la région du Lac Allard, Québec: évolution des membres mafiques et origine des gîtes massifs d'ilménite. (Unpublished PhD Thesis) University of Montréal (480 pp.).
Bolle, O., Trindade, R.I.F., Bouchez, J.L., Duchesne, J.C., 2002. Imaging downward granitic magma transport in the Rogaland Igneous Complex, SW Norway. Terra Nova 14, 87–92.
Borradaile, G.J., Jackson, M., 2004. Anisotropy of magnetic susceptibility (AMS): magnetic petrofabrics of deformed rocks. In: Martín-Hernández, F., Lüneburg, C.M., Aubourg, C., Jackson, M. (Eds.), Magnetic Fabric: Methods and Applications. Journal of the Geological Society of London, Special Publications, 238, pp. 299–360.
Bouchez, J.L., 2000. Anisotropie de susceptibilité magnétique et fabrique des granites. C. R. Acad. Sci. Paris, Sci. Terre Planèts 330, 1–14.
Brown, L.L., McEnroe, S.A., 2004. Paleomagnetism of the Egersund-Ogna anorthosite, Rogaland, Norway, and the position of Fennoscandia in the Tonian, Neoproterozoic. Geophys. J. Int. 158, 479–488.
Brown, L.L., McEnroe, S.A., 2008. Magnetic properties of anorthosites: a forgotten source for planetary magnetic anomalies? Geophys. Res. Lett. 35, L02305. http://dx.doi.org/10.1029/2007GL032522.
Bunge, H.J., 1982. Texture Analysis in Materials Sciences. Butterworths, London (559 pp.).
Carmichael, C.M., 1959. Remanent magnetism of the Allard Lake ilmenites. Nature 183, 1239–1241.
Carmichael, C.M., 1961. The magnetic properties of ilmenite–haematite crystals. Proc. R. Soc. Lond. A Math. Phys. Sci. 263, 508–530.
Carmichael, C.M., 1964. The magnetization of a rock containing magnetite and hemoilmenite. Geophysics 29, 87–92.
Čečys, A., Benn, K., 2007. Emplacement and deformation of the ca. 1.45 Ga Karlshamn granitoid pluton, southeastern Sweden, during ENE–WSW Danopolonian shortening. Int. J. Earth Sci. 96, 397–414.
Charlier, B., Sakoma, E., Sauvé, M., Stanaway, K., Vander Auwera, J., Duchesne, J.C., 2008. The Grader layered intrusion (Havre-Saint-Pierre Anorthosite, Quebec) and genesis of nelsonite and other Fe–Ti–P ores. Lithos 101, 359–378.
Charlier, B., Namur, O., Malpas, S., de Marneffe, C., Duchesne, J.C., Vander Auwera, J., Bolle, O., 2010. Origin of the giant Allard Lake ilmenite ore deposit (Canada) by fractional crystallization, multiple magma pulses and mixing. Lithos 117, 119–134.
Chevé, S., Gobeil, A., Clark, T., Corriveau, L., Perreault, S., Dion, D.J., Daigneault, R., 1999. Géologie de la région du lac Manitou (22I/14). Ministère des Ressources naturelles, Québec (RG 99-02, 69 pp.).
Corrigan, D., Hanmer, S., 1997. Anorthosites and related granitoids in the Grenville orogen: a product of convective thinning of the lithosphere? Geology 25, 61–64.
Day, R., Fuller, M., Schmidt, V.A., 1977. Hysteresis properties of titanomagnetites: grain-size and compositional dependence. Phys. Earth Planet. Inter. 13, 260–267.
Diot, H., Bolle, O., Lambert, J.M., Launeau, P., Duchesne, J.C., 2003. The Tellnes ilmenite deposit (Rogaland, South Norway): magnetic and petrofabric evidence for emplacement of a Ti-enriched noritic crystal mush in a fracture zone. J. Struct. Geol. 25, 481–501.
Dobmeier, C., 2006. Emplacement of Proterozoic massif-type anorthosite during regional shortening: evidence of the Bolangir anorthosite complex (Eastern Ghats Province, India). Int. J. Earth Sci. (Geol. Rundsch.) 95, 543–555.
Duchesne, J.C., 1999. Fe–Ti deposits in Rogaland anorthosites (South Norway): geochemical characteristics and problems of interpretation. Mineral. Deposita 34, 182–198.
Dunlop, D.J., 2002. Theory and application of the Day plot (M_{rs}/M_s versus H_{cr}/H_c). 1. Theoretical curves and tests using titanomagnetite data. J. Geophys. Res. 107 (B3), 2056.
Dunlop, D.J., Özdemir, Ö., 2009. Magnetizations in rocks and minerals. In: Kono, M. (Vol. Ed.), Schubert, G. (Series Ed.), Treatise of Geophysics, Volume 5 (Geomagnetism). Elsevier, Amsterdam, pp. 277–336.
Dymek, R.F., 2001. Observations on the Allard Lake anorthosite, Grenville Province, Quebec, and implications for petrogenesis of the CRUML belt of massif anorthosites. Geol. Soc. Am. Abstr. Programs 33, 57.
Emslie, R.F., 1978. Anorthosite massifs, rapakivi granites, and late proterozoic rifting of north America. Precambrian Res. 7, 61–98.
Emslie, R.F., Hunt, P.A., 1990. Ages and petrogenetic significance of igneous mangerite–charnockite suites associated with massif anorthosites, Grenville Province. J. Geol. 98, 213–231.
Fabian, K., Shcherbakov, V.P., McEnroe, S.A., 2013. Measuring the Curie temperature. Geochem. Geophys. Geosyst. 14. http://dx.doi.org/10.1022/2012GC004440.
Ferré, E.C., 2002. Theoretical models of intermediate and inverse AMS fabrics. Geophys. Res. Lett. 29. http://dx.doi.org/10.1029/2001GL014367.
Force, E.R., 1991. Geology of titanium-mineral deposits. Geol. Soc. Am. Spec. Pap. 259, 118.
Glazner, A.F., Miller, D.M., 1997. Late-stage sinking of plutons. Geology 25, 1099–1102.
Gobeil, A., Chevé, S., Clark, T., Corriveau, L., Perreault, S., Dion, D.J., Nabil, H., 1999. Géologie de la région du lac Nipisso (22I/13). Ministère des Ressources naturelles, Québec (RG 98-19, 60 pp.).
Gobeil, A., Brisebois, D., Clark, T., Verpaelst, P., Madore, L., Wodicka, N., Chevé, S., 2003. Géologie de la moyenne Côte-Nord. In: Brisebois, D., Clark, T. (Eds.), Géologie et ressources minérales de la partie est de la Province de Grenville. Ministère des Ressources naturelles, de la Faune et des Parcs, Québec, pp. 9–57 (DV 2002-03).
Hammond, P., 1952. Allard Lake ilmenite deposits. Econ. Geol. 47, 634–649.
Hargraves, R.B., 1959. Magnetic anisotropy and remanent magnetism in hemo-ilmenite from ore deposits at Allard Lake, Quebec. J. Geophys. Res. 64, 1565–1578.
Hargraves, R.B., 1962. Petrology of the Allard Lake anorthosite suite, Quebec. In: Engel, A.E.J., James, H.L., Leonard, B.F. (Eds.), Petrologic Studies: A Volume to Honor A.F. Buddington. Geological Society of America, Denver, pp. 163–189.

Hargraves, R.B., Burt, D.M., 1967. Paleomagnetism of the Allard Lake anorthosite suite. Can. J. Earth Sci. 4, 357–369.
Hébert, C., Cadieux, A.M., van Breemen, O., 2005. Temporal evolution and nature of Ti–Fe–P mineralization in the anorthosite–mangerite–charnockite–granite (AMCG) suites of the south-central Grenville Province, Saguenay–Lac St. Jean area, Quebec, Canada. Can. J. Earth Sci. 42, 1865–1880.
Henry, B., 1997. The magnetic zone axis: a new element of magnetic fabric for the interpretation of the magnetic lineation. Tectonophysics 271, 325–331.
Hext, G.R., 1963. The estimation of second-order tensors, with related tests and design. Biometrika 50, 353–373.
Higgins, M.D., 2011. Textural coarsening in igneous rocks. Int. Geol. Rev. 53, 354–376.
Higgins, M.D., van Breemen, O., 1996. Three generations of anorthosite–mangerite–charnockite–granite (AMCG) magmatism, contact metamorphism and tectonism in the Saguenay–Lac St. Jean region of the Grenville Province, Canada. Precambrian Res. 79, 327–346.
Hocq, M., 1982. Région du Lac Allard. Ministère de l'Energie et des Ressources, Québec (DPV-894, 99 pp.).
Huang, F., Lundstrom, C.C., Glessner, J., Ianno, A., Boudreau, A., Li, J., Ferré, E.C., Marshak, S., DeFrates, J., 2009. Chemical and isotopic fractionation of wet andesite in a temperature gradient: experiments and models suggesting a new mechanism of magma differentiation. Geochim. Cosmochim. Acta 73, 729–749.
Indares, A., Martignole, J., 1993. Etude régionale du Supergroupe de Wakeham, moyenne Côte-Nord. Ministère de l'Energie et des Ressources, Québec (MB 91-21, 73 pp.).
Jelinek, V., 1981. Characterization of the magnetic fabrics of rocks. Tectonophysics 79, T63–T67.
Kontny, A., Engelmann, R., Grimmer, J.C., Greiling, R.O., Hirt, A., 2012. Magnetic fabric development in a highly anisotropic magnetite-bearing ductile shear zone (Seve Nappe Complex, Scandinavian Caledonides). Int. J. Earth Sci. (Geol. Rundsch.) 101, 671–692.
Launeau, P., Robin, P.Y.F., 1996. Fabric analysis using the intercept method. Tectonophysics 267, 91–119.
Launeau, P., Robin, P.Y.F., 2005. Determination of fabric and strain ellipsoids from measured sectional ellipses — examples. J. Struct. Geol. 27, 2223–2233.
Madore, L., Verpaelst, P., Brisebois, D., Hocq, M., Dion, D.J., Lavallée, G., Choinière, J., 1999. Géologie de la région du lac Allard (12L/11). Ministère des Ressources naturelles, Québec (RG 98-01, 37 pp.).
McBirney, A.R., Nicolas, A., 1997. The Skaergaard layered series. Part II. Magmatic flow and dynamic layering. J. Petrol. 38, 569–580.
McEnroe, S.A., Robinson, P., Langenhorst, F., Frandsen, C., Terry, M.P., Boffa Ballaran, T., 2007. Magnetization of exsolution intergrowths of hematite and ilmenite: mineral chemistry, phase relations, and magnetic properties of hemo-ilmenite ores with micron- to nanometer-scale lamellae from Allard Lake, Quebec. J. Geophys. Res. 112, B10103.
McLelland, J.M., Selleck, B.W., Hamilton, M.A., Bickford, M.E., 2010. Late- to post-tectonic setting of some major Proterozoic anorthosite–mangerite–charnockite–granite (AMCG) suites. Can. Mineral. 48, 729–750.
Morisset, C.E., Scoates, J.S., Weis, D., Friedman, R.M., 2009. U–Pb and $^{40}Ar/^{39}Ar$ geochronology of the Saint-Urbain and Lac Allard (Havre-Saint-Pierre) anorthosites and their associated Fe–Ti oxide ores, Québec: evidence for emplacement and slow cooling during the collisional Ottawan orogeny in the Grenville Province. Precambrian Res. 174, 95–116.
O'Driscoll, B., Hargraves, R.B., Emeleus, C.H., Troll, V.R., Donaldson, C.H., Reavy, R.J., 2007. Magmatic lineations inferred from anisotropy of magnetic susceptibility fabrics in Units 8, 9, and 10 of the Rum Eastern Layered Series, NW Scotland. Lithos 98, 27–44.
Passchier, C.W., Trouw, R.A.J., 2005. Microtectonics, 2nd ed. Springer-Verlag, Berlin, Heidelberg (xvi + 366 pp.).
Paterson, S.R., Vernon, R.H., 1995. Bursting the bubble of ballooning plutons: a return to nested diapirs emplaced by multiple processes. Geol. Soc. Am. Bull. 107, 1356–1380.
Pignotta, G.S., Benn, K., 1999. Magnetic fabric of the Barrington Passage pluton, Meguma Terrane, Nova Scotia: a two stage fabric history of syntectonic emplacement. Tectonophysics 307, 75–92.
Plissart, G., Diot, H., Monnier, C., Mărunţiu, M., Berger, J., 2012. Relationship between a syntectonic granitic intrusion and a shear zone in the Southern Carpathian–Balkan area (Almăj Mountains, Romania): implications for late Variscan kinematics and Cherbelezu granitoid emplacement. J. Struct. Geol. 39, 83–102.
Prior, D.J., Boyle, A.P., Brenker, F., Cheadle, M.C., Day, A., Lopez, G., Peruzzo, L., Potts, G.J., Reddy, S., Spiess, R., Timms, N.E., Trimby, P., Wheeler, J., Zetterström, L., 1999. The application of electron backscatter diffraction and orientation contrast imaging in the SEM to textural problems in rocks. Am. Mineral. 84, 1741–1759.
Rivers, T., 2008. Assembly and preservation of lower, mid, and upper orogenic crust in the Grenville Province — implications for the evolution of large hot long-duration orogens. Precambrian Res. 167, 237–259.
Rivers, T., 2012. Upper-crustal orogenic lid and mid-crustal core complexes: signature of a collapsed orogenic plateau in the hinterland of the Grenville Province. Can. J. Earth Sci. 49, 1–42.
Rivers, T., Culshaw, N., Hynes, A., Indares, A., Jamieson, R.A., Martignole, J., 2012. The Grenville Orogen – A Post-LITHOPROBE Perspective. In: Percival, J.A., Cook, F.A., Clowes, R.M. (Eds.), Tectonic Styles in Canada: The LITHOPROBE Perspective. Geological Association of Canada, Special Publication, 49, pp. 97–236.
Robinson, P., Harrison, R.J., McEnroe, S.A., Hargraves, R., 2002. Lamellar magnetism in the hematite–ilmenite series as an explanation for strong remanent magnetization. Nature 418, 517–520.
Robinson, P., Heidelbach, F., Hirt, A.M., McEnroe, S.A., Brown, L.L., 2006. Crystallographic–magnetic correlations in single-crystal haemo-ilmenite: new evidence for lamellar magnetism. Geophys. J. Int. 165, 17–31.
Robinson, P., Fabian, K., McEnroe, S.A., Heidelbach, F., 2013. Influence of lattice-preferred orientation with respect to magnetizing field on intensity of remanent magnetization in polycrystalline hemo-ilmenite. Geophys. J. Int. 192, 514–536.
Rochette, P., 1987. Magnetic susceptibility of the rock matrix related to magnetic fabric studies. J. Struct. Geol. 9, 1015–1020.
Rochette, P., Jackson, M., Aubourg, C., 1992. Rock magnetism and the interpretation of anisotropy of magnetic susceptibility. Rev. Geophys. 30, 209–226.
Sakoma, E.M., Martin, R.F., 2002. Oxidation-induced postmagmatic modifications of primary ilmenite, NYG-related aplite dyke, Tibchi complex, Kalato, Nigeria. Mineral. Mag. 66, 591–604.
Streckeisen, A., 1974. How Should Charnockitic Rocks Be Named? In: Bellière, J., Duchesne, J.C. (Eds.), Société Géologique de Belgique, Liège, pp. 349–360 (Volume du Centenaire).
Tollo, R.P., Corriveau, L., McLelland, J., Bartholomew, M.J., 2004. Proterozoic tectonic evolution of the Grenville orogen in North America: an introduction. In: Tollo, R.P., Corriveau, L., McLelland, J., Bartholomew, M.J. (Eds.), Proterozoic Tectonic Evolution of the Grenville Orogen in North America. Geological Society of America Memoir, 197, pp. 1–18.
Uyeda, Y., Fuller, M.D., Belshé, J.C., Girdler, R.W., 1963. Anisotropy of magnetic susceptibility of rocks and minerals. J. Geophys. Res. 68, 279–291.
van Breemen, O., Higgins, M.D., 1993. U–Pb zircon age of the southwest lobe of the Havre-Saint-Pierre Anorthosite Complex, Grenville Province, Quebec. Can. J. Earth Sci. 30, 1453–1457.
Vander Auwera, J., Weis, D., Duchesne, J.C., 2006. Marginal mafic intrusions as indicators of downslope draining of dense residual melts in anorthosite diapirs? Lithos 89, 329–352.
Verpaelst, P., Madore, L., Brisebois, D., Hocq, M., Dion, D.J., Lavallée, G., Choinière, J., 1999. Géologie des régions du lac Jérôme, du lac Sanson et de la Petite Rivière de l'Abbé-Huard (12L/13, 12L/14, 12M/03). Ministère des Ressources naturelles, Québec (RG 98-02, 38 pp.).
Wodicka, N., David, J., Parent, M., Gobeil, A., Verpaelst, P., 2003. Géochronologie U–Pb et Pb–Pb de la région de Sept-Iles — Natashquan, Province de Grenville, moyenne Côte-Nord. In: Brisebois, D., Clark, T. (Eds.), Géologie et ressources minérales de la partie est de la Province de Grenville. Ministère des Ressources naturelles, de la Faune et des Parcs, Québec, pp. 59–117 (DV 2002-03).
Woodcock, N.H., Naylor, M.A., 1983. Randomless testing in three-dimensional orientation data. J. Struct. Geol. 5, 539–548.